BL7B

Scintillation and Luminescence Properties of Sn^{2+}-doped Oxide Glass[1]

H. Masai[1], T. Yanagida[2], Y. Fujimoto[2], M. Koshimizu[3], T. Yoko[1] and K. Asai[3]

[1]*Institute for Chemical Research, Kyoto University, Kyoto 611-0011, Japan*

[2]*Kyushu Institute of Technology, Kitakyushu 808-0196, Japan*

[3]*Department of Applied Chemistry, Graduate School of Engineering, Tohoku University, Sendai 980-8579, Japan*

RE (rare-earth)-free phosphors have long been developed in terms of abundance as natural resource. Among them, RE-free glasses have advantage that various kinds of elements can be incorporated to control the emission properties. One application of the RE-free glasses may be scintillators, because most of conventional scintillators include RE ions as luminescent centers and as the constituent of the host matrix. In this study, we demonstrated the applicability of RE-free glasses for scintillators.

The SnO-SrO-B_2O_3 and SnO-ZnO-P_2O_5 glass samples were fabricated by a conventional melt-quenching technique. The raw materials were melted in platinum crucibles, and subsequently were quenched on a stainless steel at 473 K. The glass samples were annealed at the glass transition temperatures.

The pulse height spectra of the α-ray from ^{241}Am were obtained for the scintillation detectors quipped with sample scintillators. The emission and excitation spectra of samples were measured at room temperature under the irradiation of synchrotron radiation having energies of 6–20 eV at the UVSOR facility (BL7B).

Figure 1 shows the pulse height spectra of the samples. Because the experimental set up and the excitation source was the same for each sample, the multichannel analyzer (MCA) channel is roughly proportional to the number of photoelectrons. A clear peak was observed for each sample. This result indicates that the light yield was sufficient for detection of ionizing radiation whose energy is on the order of MeV, although the light yield was significantly smaller than that of Li-glass.

Figure 2 shows contour plot of emission and excitation spectra of the $0.5SnO$-$24.5SrO$-$75B_2O_3$ and $5.0SnO$-$60ZnO$-$40P_2O_5$ glass. Each contour plot shows the photon energy of excitation (ordinate) and emission (abscissa), and the intensity axes are shown on an identical linear scale. We observed two excitation bands; one is the band at ~6 eV corresponding to the S_0-S_2 transition of Sn^{2+}. We observed another peak at above 20 eV. Assuming that this band corresponds to the excitation in the host glass, the emission occurs via the energy transfer from the host to the Sn^{2+} center. The observation of the high-energy band suggests that effective scintillation occurs, because the energy transfer is essential in obtaining effective scintillation.

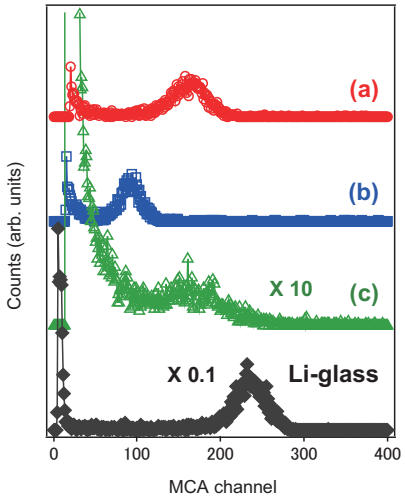

Fig. 1. Pulse-height spectra of the samples for ^{241}Am α-ray; (a): $5SnO$-$60ZnO$-$40P_2O_5$, (b): $0.5SnO$-$24.5SrO$-$75B_2O_3$, (c): $0.1SnO$-$24.9SrO$-$75B_2O_3$.

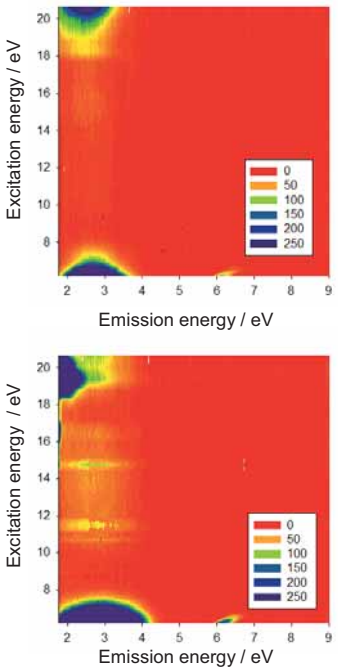

Fig. 2. Contour plot of emission and excitation spectra of the $5.0SnO$-$60ZnO$-$40P_2O_5$ (lower) and $0.5SnO$-$24.5SrO$-$75B_2O_3$ (upper).

[1] Hirokazu Masai, *et al.*, Appl. Phys. Lett., **101** (2012) 191906.

BL2A

Mo L_{III}-Edge XANES Study of MoO_3-Modified H-GaAlMFI Catalysts for Methane Dehydroaromatization

H. Aritani[1], T. Sugawara[1], N. Naijo[1], K. Takanashi[1], S. Mogi[1] and A. Nakahira[2]
[1]*Department of Life Science & Green Chemistry, Saitama Institute of Technology, Fukaya 369-0293, Japan*
[2]*Graduate School of Engineering, Osaka Prefecture University, Sakai 599-8531, Japan*

MoO_3-modified H-MFI (Mo/H-MFI) is a typical catalyst for methane dehydroaromatization, which is an important reaction for direct GTL (Gas to Liquid) processes. The H-MFI zeolite (SiO_2/Al_2O_3=28-40) shows unique properties for dehydroaromatization of light alkanes such as propane and ethane. The catalytic activity is based on strong acidity and selective sieving effects. By MoO_3 modification, it shows high activity for methane dehydro-aromatiozation (MTB reaction). In this reaction, MoO_x species are reduced and carbonized to form Mo_2C-like carbide species. The carbide species plays a key role in methane dehydrogenation. As a same time, carbon contamination on Mo/H-MFI proceeds. It is a major source for catalytic deactivation. Because the deactivation relates to the strong acidity on H-MFI, an improvement of H-MFI support is called for. In the present study, Ga-containing H-MFI (GaAl-MFI) supports have been synthesized hydrothermally [1], and MoO_x-modified GaAl-MFI catalysts have been applied to employ the methane dehydroaromatization. By substitution of Ga ions onto H-MFI framework, the acidity weakens slightly. The effect of Ga ion onto H-MFI, highly active and durable catalysts can be expected. In the present report, Mo species on GaAl-MFI catalysts have been characterized by Mo L_{III}-edge XANES to evaluate the carbide species after the MTB reaction.

Catalysts were prepared by impregnation of H-GaAlMFI support with $MoO_2(acac)_2$–$CHCl_3$ solution, and followed by drying overnight and calcination at 773 K for 3 h. The amount of MoO_3-loading is 5.0 wt% in this study. H-GaALMFI supports were synthesized hydrothermally at 413 K for a week, and followed by ion-exchanging with NH_4Cl and calcination at 873 K. The catalytic activity of methane dehydroaromatization was evaluated by means of fixed bed flow reaction, as described in a separate paper [2]. The catalyst samples are denoted as Mo/Ga*m*MFI*n*, in which *m*=Ga/Al and n=Si/Al_2 atomic ratios. Mo L_{III}-edge XANES spectra were measured in BL2A of UVSOR-IMS in a total-electron yield mode using InSb double-crystal monochromator. Photon energy was calibrated by using Mo metal-foil at Mo L_{III}-edge, and normalized XANES spectra and their second derivatives are presented. REX-2000 (Rigaku) software was used by normalization of each XANES spectrum.

Figure 1 shows the Mo/H-MFI28(Ga-free), Mo/GaAl-MFI28 (intraframework Ga onto MFI with Ga/Al=10-50), and Mo-Ga/H-MFI28 (Ga_2O_3-MoO_3 co-impregnation) catalysts after MTB reaction. For all the catalysts, the edge energy values of L-XANES are lower than bare Mo_2C, suggesting the formation of micro-particles which consist of metallic and carbonized Mo. Mo/H-Ga50MFI28 shows the maximum reactivity for MTB reaction, and thus, Ga ions do not affect the Mo carnbonization. Mo-Ga interaction can not be seen in both the structural evaluation and catalytic properties. It is concluded that formation of active Mo carbide species proceeds independently of Ga modification.

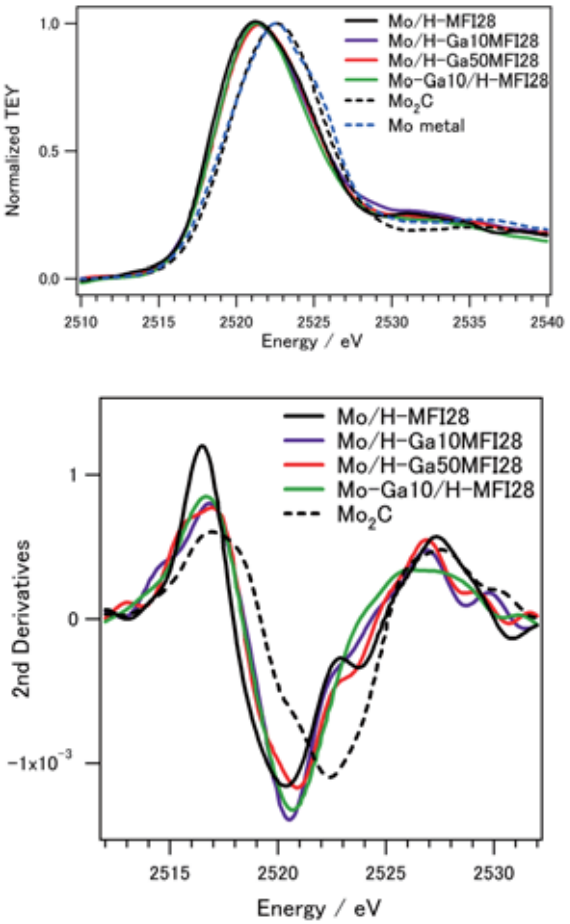

Fig. 1. Mo L_{III}-edge XANES spectra (top) and their second derivatives (bottom) over MoOx- modified GaAl-MFI catalysts after MTB reaction.

[1] K. Nagashima, S. Nakamura, K. Okada, A. Nakahira and H. Aritani, Bull. Chem. Soc. Jpn. **82** (2009) 1203.
[2] H. Aritani, H. Shibasaki, H. Orihara and A. Nakahira, J. Environm. Sci. **21** (2009) 736.

BL2A

Local Structure of Na-K and K-K edge of Artificial Zeolites Prepared from Blast Furnace Slag

M. Sato[1], K. Kumadani[2], T. Shirai[2] and A. Nakahira[1, 2]

[1]*Kansai Center for Industrial Materials Research, Tohoku University, Osaka 599-8531, Japan*

[2]*Department of Material Science and Engineering, Osaka Prefecture University, Osaka 599-8531, Japan*

The depletion of natural resources is one of the our serious problems. Therefore, the development of the novel recycling technology has been performed energetically. Blast furnace slag (BF slag) is one of the waste materials that the development and establishment of the effective recycling technology and system become the urgent assignment. The BF slag has been produced approximately 25 million tons per year, and it is recycled as Portland cement, base coarse materials, fine aggregate for concrete and ground improvement materials, and so on. However, recycling rate of BF slag is insufficient by comparing to the amount of generation. In this study, A and Y type zeolite were prepared using BF slag as a starting material to reduce an emission of waste materials, and local structure of Na-K and K-K edge of products were measured in order to investigate the condition of exchanged cation in zeolite.

BF slag and sodium aluminate were used as starting materials. Firstly, BF slag was ground to become their particle size less than 70 μm. Ground slag powder was undergone an acid treatment to remove Ca component. Then, Ca removed slag powder was hydrothermally treated in NaOH solution at 368 K. In this study, the ratio of Si to Al was changed in the range from 0.5 to 2.4 by addition of sodium aluminate. Obtained samples were ion exchanged in 1000 ppm KNO_3 solution at room temperature for several periods. K-K edge XANES spectra of obtained samples were measured by a total electron yield mode at room temperature using InSb double-crystal monochrometer, and Na-K edge XANES spectra was also measured by a total electron yield mode at room temperature using Beryl double-crystal monochrometer at BL-2A station of UVSOR.

Figure 1 shows Na-K edge XANES spectra of A type zeolite prepared from BF slag before and after ion exchange. Commercial A type zeolite and A type zeolite prepared using reagents were used as references. The position of second peak around 1080 eV was different between references and sample. This result shows that Na environment in zeolite prepared from BF slag more distorts than references [1].

In the case of K-K edge XANES spectra of A type zeolite prepared from BF slag after ion exchange. Although clear spectra did not obtain for the sample ion exchanged for 5 and 30 min, obtained spectra were similar spectra with zeolite 3A, which is the potassium form of the type A crystal structure. This result shows that exchanged K^+ ions in zeolite prepared from BF slag exist in similar environment with zeolite 3A.

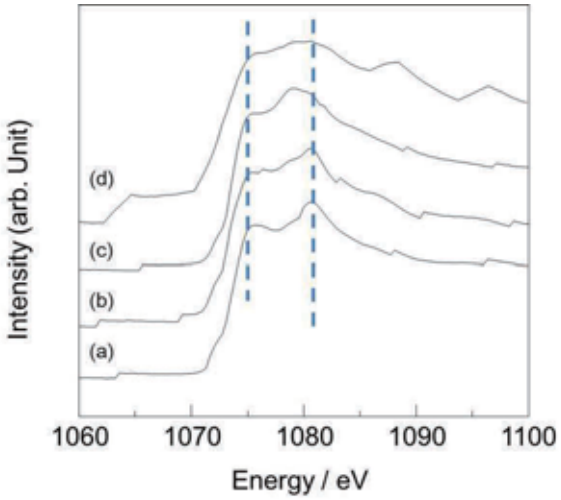

Fig. 1. Na-K edge XANES spectra of A type zeolite prepared from BF slag and references. (a) Commercial A type zeolite, (b) A type zeolite prepared using reagents, (c) A type zeolite prepared from BF slag, (d) after ion exchange for 30 min.

[1] D. R. Neuville, L. Cormire, A-M. Flank, R. J. Prado and P. Lagarde, Eur. J. Mineral **16** (2004) 809-816.

BL2A

Investigation of Local Structure of P-K edge of Fe doped Amorphous Calcium Phosphate Powders

M. Sato[1], T. Nagayasu[2], S. Hayashi[2] and A. Nakahira[1, 2]

[1]*Kansai Center for Industrial Materials Research, Tohoku University, Osaka 599-8531, Japan*

[2]*Department of Material Science and Engineering, Osaka Prefecture University, Osaka 599-8531, Japan*

Hydroxyapatite ($Ca_{10}(PO_4)_6(OH)_2$, HAp) has been well understood as an alternate materials of our hard tissue because of their excellent osteoconductivity and biocompatibility. Besides, HAp also has good protein adsorption ability and ion exchange ability. Therefore, many studies for bioactivity and degradable behavior of Mg, Mn, Fe, Si, Zn doped HAp have been performed.

In a previous study, we prepared Fe doped HAp powders by co-precipitation and hydrothermal method, and investigated the effect of Fe addition on the crystal phase, microstructure, local structure around Fe, Ca and P atoms and other properties [1, 2]. From the result of XAFS measurement, it was suggested that the added Fe mainly existed as α-FeOOH and α-Fe_2O_3 phase, and small amount of Fe was substituted into the HAp structure. Since the generation of α-FeOOH phase is caused by the alkali condition of preparation method, sol-gel method, which does not require the alkali condition and typical method to obtain amorphous calcium phosphate, was used as a preparation method.

Metal Ca, phosphoric acid and Fe acetylacetonate were used as starting materials. These were mixed up in ethanol solution at 353 K for 4 hours becoming the Ca/P ratio of 1.67 and the ratio of Fe from 1 to 10 mol% for Ca. After that, they were filtered and dried at 323 K for overnight. P-K edge XANES spectra of obtained HAp powders were measured in a total electron yield mode at room temperature using InSb double-crystal monochrometer at BL-2A station of UVSOR.

Figure 1 shows P-K edge XANES spectra of Fe doped amorphous calcium phosphate powders prepared by sol-gel method. Commercial HAp was used as a reference. The obtained spectra of Fe doped sample showed similar spectra independent from the ratio of Fe. This result indicates that the local structure around P atom of Fe doped samples does not change by Fe addition. Besides, clear peak shift to high energy site and spectrum broadening were observed by comparison with the commercial HAp.

From these results, it is suggested that relatively higher amount of Fe can be doped than our previous studies [1, 2], and this data is important to clarify the condition and solid solubility limit of Fe in the HAp structure.

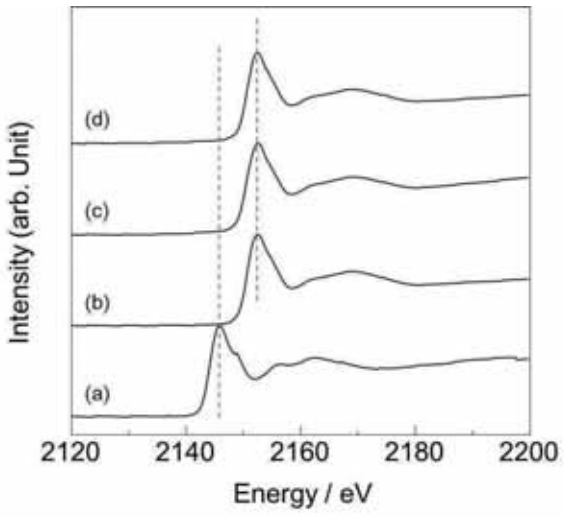

Fig. 1. P-K edge XANES spectra of Fe doped amorphous calcium phosphate powder prepared by sol-gel method.

[1] M. Sato, S. Yamamoto, Y. Nishio, Y. Takamatsu and A. Nakahira, UVSOR Activity Report **38** (2011) 115.

[2] M. Sato, Y. Kawabe, S. Misu, S. Hayashi and A. Nakahira, UVSOR Activity Report **39** (2012) 81.

BL2A

Study of the Local Strucures of LTA-type Zeolite Nanopowder by XANES Evaluations

A. Nakahira[1, 2], T. Tagami[1], T. Shirai[1], M. Sato[2], T. Nagayasu[1] and H. Aritani[3]

[1]*Faculty of Engineering, Osaka Prefecture University, Gakuencho, Sakai 599-8531, Japan*

[2]*Osaka Center, IMR, Tohoku University, Gakuencho, Sakai 599-8531, Japan*

[3]*Saitama Institute of Technology, Fukaya 369-0293, Japan*

It is well-known that zeolites are microporous, aluminosilicate minerals commonly used as various commercial adsorbents. In fact, zeolites are widely used in industry for water purification, as catalysts, for the preparation of advanced materials and Cs purification in nuclear reprocessing. In addition, they purification are used to extract nitrogen from air to increase oxygen content for both industrial and medical purposes. However, the modification of microstructures and morphology is needed for zeolites to expand their applications in various industrial fields. [1-3]

Recently, as one approach for the modification of microstructures and morphology of zeolites, much attention are paid to the synthesis of the finely nanosized zeolite powders by the novel processing. Various processing are attempted to synthesize the nanosized zeolite powders.

In this study, the finely nanosized zeolite powders were synthesized by the mechanical mixing processing with high energy grinding forces and the local structures were investigated for finely nanosized zeolite powders prepared by the mechanical mixing processing.

Zeolite was synthesized by the following method. LTA type zeolites were synthesized at 60 ℃ to 90 ℃ by the soft chemical solution processing using sodium silicate as s silicon source and aluminum silicate as an aluminum source. The mixture of sodium silicate and aluminum silicate was aged for 12h and then treated under hydrothermal conditions for 12 h to 48 h without stirring. The solid product was filtered, frequently washed, and air-dried at room temperature. Subsequently, the powder of this LTA type zeolites powder was milled by the mechanical milling method with the high energy forces for 1h to 24 h. After the milled and ground nanosized LTA type zeolite powder were characterized by Xrd method and TG/DTA. The microstructures of nanosized LTA type zeolite powder were observed by scanning electron microscopy. The local structures around Al for the products of nanosized LTA type zeolite powder were characterized by measuring X-ray adsorption near edge structure (XANES) at BL2A in UVSOR.

The results of XRD for synthesized zeolite indicated that the obtained products were LTA type zeolites. XRD results showed that after the mechanical mixing processing for 2 hs the ground products were also identified to be LTA type. Products obtained after the mechanical mixing processing had the average particle of a few hundred nanometer in diameter. Suggesting the nanosized LTA zeolite powders were successfully obtained by after the mechanical mixing processing for 2 hs.

Fig.1 shows the XANES spectra of zeolites and reference materials. As shown in Fig. 1, XANES spectra of sample obtained after the mechanical mixing processing for 2h the same spectra as the LTA without mechanical mixing. These results suggest nanosized LTA zeolite powders possess the good crystallinity and also the same local structure of Al after the mechanical mixing processing.

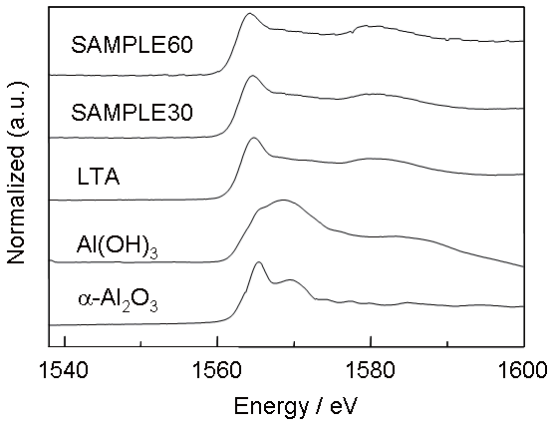

Fig. 1. Al XANES spectra of zeolites and reference materials.

[1] M. E. Davis and R. F. Lobo, Chem. Mater., **4** (192) 756.

[2] A. Nakahira, S. Nishimura, H. Aritani, T. Yamamoto and S. Ueda, J. Mater. Sci. **36** (2001) 1885.

[3] A. Nakahira, S. Yamamoto, M. Sato, Y. Takamatsu, S. Misu, Y. Kawabe, Y. Nishio and H. Aritani, UVSOR Activity Report **38** (2011) 112.

BL2A

XANES Evaluation of Zeolites obtained from Waste Glass

A. Nakahira[1, 2], T. Tagami[1], T. Shirai[1], K. Kumadani[1], M. Sato[2] and H. Aritani[3]

[1]*Faculty of Engineering, Osaka Prefecture University, Gakuencho, Sakai 599-8531, Japan*

[2]*Osaka Center, IMR, Tohoku University, Gakuencho, Sakai 599-8531, Japan*

[3]*Saitama Institute of Technology, Fukaya 369-0293, Japan*

Glass is widely used in many fields and an ideal material for recycle, whereas it is used for new glass container manufacture it is virtually infinitely recyclable. The glass component in municipal waste is usually made up of bottles, broken glassware, light bulbs and other items. Glass makes up a large component of household and industrial waste. The use of the recycled glass as aggregate in concrete and others has become popular in modern times, although large scale researches have been carried out long year. It is expected that glass recycling is the process of turning waste glass into usable products because the use of recycled glass in new containers helps save energy. In fact, recycling of waste glass and other sources help in brick and ceramic manufacture, and it conserves raw materials, reduces energy consumption [1-4].

As one approach of the recycle of waste glass, much attention are paid to the synthesis of zeolites for waste glass by soft chemical processing, that is, eco-processing with low environmental load. Especially, the finely zeolite powders are expected to synthesize by the novel soft chemical eco-processing. Various eco-soft chemical processing with low environmental load are attempted to synthesize the novel zeolites.

In this study, the finely LTA zeolite powders were synthesized by the novel soft chemical eco-processing with low environmental load and the local structures were investigated for zeolite powders prepared by the novel eco-soft chemical processing with low environmental load.

Glass was prepared from the waste glass, such as a window sheet glass. Zeolite was synthesized by the following eco-soft chemical processing with low environmental load. LTA type zeolites were synthesized at 90 °C by the eco-recycle soft chemical processing using sodium silicate as s silicon source and aluminum silicate as an aluminum source. The mixture of both sodium silicate and aluminum silicate was aged for 24h and then heat-treated under hydrothermal conditions for 48 h with magnetic stirring. The solid product was filtered, frequently washed, and air-dried at room temperature. Subsequently, the powder of the zeolite was milled by the mortar. The solid products were evaluated by XRD method and TG/DTA equipments. The microstructures of the solid product powder were observed by scanning electron microscopy (SEM). The local structures around Si for the products of the solid product powder were characterized by measuring X-ray adsorption near edge structure (XANES) at BL02A in UVSOR.

The results of XRD indicated that the products synthesized under the optimum synthetic conditions were identified to be a LTA type zeolite without other phase, although some products contained LTA and other phases. These results suggest that the fine LTA zeolite powders were successfully obtained from waste glass by eco-soft chemical processing with low environmental load.

The XANES spectra of products and reference materials are shown in Fig.1. XANES spectra of sample obtained the same spectra as the commercial LTA. These results suggest the fine LTA zeolite powders possess the good crystallinity and also the same local structure of Si as the commercial LTA (com LTA).

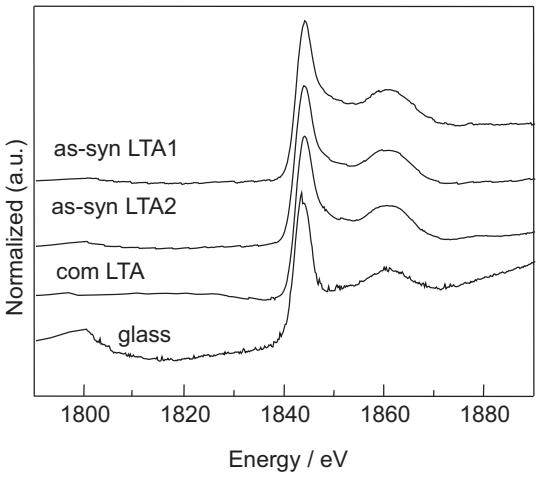

Fig. 1. Si XANES spectra of zeolites and reference materials.

[1] Y. Shaoa, T. Leforta, S. Morasa and D. Rodriguezb, Cement and Concrete Research. **30** (2000) 91.

[2] A. R. Boccaccini, M. Bücker, J. Bossert and K. Marszalek, Waste Management. **17** (1997) 39.

[3] A. Nakahira, S. Yamamoto, M. Sato, Y. Takamatsu, S. Misu, Y. Kawabe, Y. Nishio and H. Aritani, UVSOR Activity Report. **38** (2010) 112.

[4] M. Sato, S. Yamamoto, Y. Nishio, Y. Takamatsu, K. Kumadani and A. Nakahira, UVSOR Activity Report . **38** (2010) 114.

BL3B

Photoluminescence of Si-O-C(-H) Ceramics Derived from Polysiloxanes

T. Kawai[1] and M. Narisawa[2]

[1] *Graduate School of Science, Osaka Prefecture University, Sakai 599-8531, Japan*

[2] *Graduate School of Engineering, Osaka Prefecture University, Sakai 599-8531, Japan*

The photoluminescence (PL) properties of Si-O-C materials derived from organosilicon polymers have been attracting widespread attention in recent years [1, 2]. Simple chemical composition of such Si-O-C without special activator was promising for use in light-emitting diode (LED) systems. Though some Si-O-C transparent materials were synthesized by sol-gel methods or CVD methods, the precise adjustment of resulting chemical composition was not easy in such sol-gel or CVD methods. Recently, we succeeded in synthesizing Si-O-C(-H) ceramics with a white appearance by using hydrogen in the pyrolysis process for silicone resin particles [3, 4]. In this study, we have investigated the PL properties of the Si-O-C(-H) ceramics decarbonized at different temperatures.

Figure 1 shows the PL spectra of the Si-O-C(-H) ceramic decarbonized at 750 °C. Under excitation on the shorter wavelength than 240 nm, the broad PL bands are observed around 320 and 450 nm. The 450 nm bands have a long tail on the longer wavelength region. On the other hand, the excitation on the longer wavelength than 250 nm induces the broad PL bands peaking at 420 nm and having a shoulder structure around 540 nm. The shape of the PL bands indicates that the Si-O-C(-H) ceramic decarbonized at 750 °C has several PL centers.

Figure 2 shows the PL spectra of the Si-O-C(-H) ceramics decarbonized at 1100 °C under excitation at various wavelength. The broad PL bands with a peak at 500 nm are observed. The peak energy and band-shape of the PL bands are independent of the excitation wavelength. The fact indicates that the decarbonization at 1100 °C leads to the transformation to the more stable PL centers.

In the simple chemical composition of Si-O-C(-H), the oxygen deficiency centers called ODC (II) are often proposed as possible PL centers. The excitation and emission due to the transition between S_0 (singlet ground state) and S_1 (singlet excited state) in ODC (II) occur around 5.0 eV (245 nm) and 4.3 eV (290 nm), respectively [5]. Since the 320 nm PL band of the Si-O-C(-H) ceramic decarbonized at 750 °C appears only under excitation on the shorter wavelength than 240 nm, the 320 nm PL band would be attributed to the $S_1 \rightarrow S_0$ radiative transition in ODC(II). On the other hand, the 450 nm PL band might come from the transition between S_0 and T_1 (triplet excited state) in ODC (II). The appearance of the 450 nm PL band under excitation on the shorter wavelength than 240 nm implies the existence of transfer from the S_1 to T_1 states. In order to obtain information on the PL centers of the Si-O-C(-H) ceramics, the shape of the PL bands is carefully analyzed.

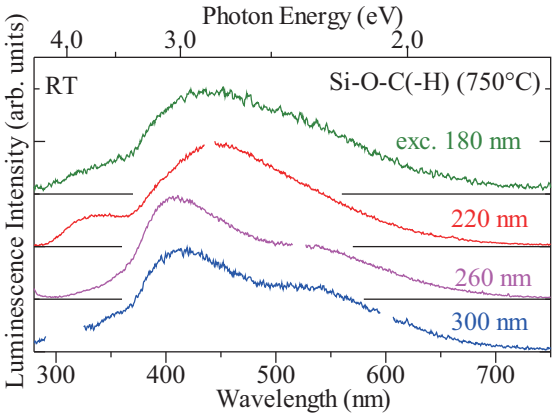

Fig. 1. Luminescence spectra of the Si-O-C(-H) ceramics decarbonized at 800 °C.

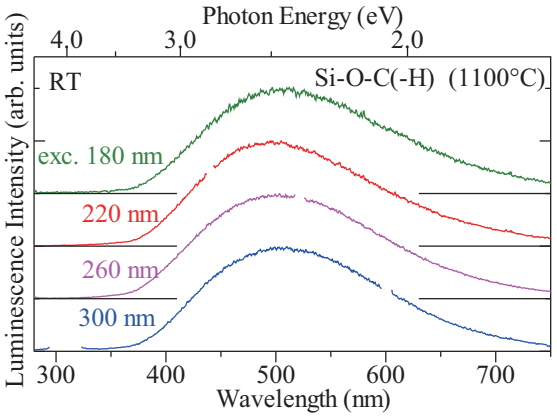

Fig. 2. Luminescence spectra of the Si-O-C(-H) ceramics decarbonized at 1100 °C.

[1] A. Karakuscu *et al.*, J. Am. Ceram. Soc. **92** (2009) 2969.

[2] S. Gallis *et al.*, Appl. Phys. Lett. **97** (2010) 081905.

[3] M. Narisawa *et al.*, Bull. Chem. Soc. Jpn. **85** (2012) 724726.

[4] M. Narisawa *et al.*, J. Am. Ceram. Soc. **95** (2012) 3935.

[5] L. Skuja: J. Non-Cryst. Solids **239** (1998) 16.

BL3B

Intrinsic Luminescence and Host Sensitization of Rare-earth Ions in Lanthanum Scandium Borate upon VUV Excitation

N. Kodama, Y. Morisawa, A. Abe, T. Sakashita and T. Takahashi

Faculty of Engineering and Resource Science, Akita University, Akita 010-8502, Japan

Host sensitization of rare-earth ions (RE^{3+} = Gd^{3+} and Ce^{3+}) has been observed in some phosphates and borates [1-3]. The intrinsic luminescence characteristics of lanthanum scandium borate, $LaSc_3(BO_3)_4$ (LSB) were investigated, in which the absorption of vacuum ultraviolet (VUV) light by the host may facilitate efficient energy transfer to Re^{3+} ions. Here, energy transfer was observed from the self-trapped exciton (STE) to Sm^{3+} and Tb^{3+} ions.

Emission and excitation spectra were measured at temperatures in the range of 7.8-293 K using the UVSOR facility. Figures 1(a) and (b) show emission spectra observed for an undoped LSB polycrystal with various excitation wavelengths at 293 and 7.8 K. The emission spectrum with VUV excitation at 70 and 160 nm consists of three intrinsic broad bands at 253, 323, and 379 nm. The feature of the emission spectrum for a LSB single crystal is the same as that for the polycrystal. Figure 2 shows excitation spectra at 293 K for both the LSB polycrystal and single crystal, which consist of fairly broad bands between 50 and 215 nm. The band edge of the single crystal is observed around 215 nm and the broad bands are assigned as bandgap excitations or molecular transitions of the BO_3^{3-} group. Both the single crystal and polycrystal spectra exhibit the same features with a sharp rise below 215 nm.

The three intrinsic emissions can be assigned to recombination of the distinct STEs (I, II, and III) that could be associated with bandgap excitations or molecular transitions of the BO_3^{3-} group. The decay times of the emissions, I (253 nm), II (323 nm) and III (379 nm) are less than 10 ns, 115 ns, and 3.4 μs, respectively. By analogy with the STE states in alkali halides [4], the I (fast) and II (fast) STE emissions originate from singlet transitions on center and off-center configurations, respectively, whereas the III (slow) STE emission is suggested to originate from a triplet transition on the off-center configuration. The emission spectra of undoped LSB, Sm^{3+}-doped LSB polycrystals (LSB:Sm), and Tb^{3+}-doped LSB polycrystals (LSB:TB) excited at 70 and 160 nm at 296 K are shown in Figs. 3(a)-(c).

For LSB:Sm, the intrinsic emissions (STE emission) decrease with increase in the Sm^{3+} concentration (1-30 at.%) (Fig. 3(a)) and this is accompanied by the appearance of intense emissions from the $^4G_{5/2}\rightarrow{}^6H_J$ transitions of Sm^{3+} (Fig. 3(b)). This suggests efficient energy transfer from the STE to Sm^{3+} ions. The Sm^{3+} emission intensity passes through a maximum at 3-5 at.% with increasing Sm^{3+} concentration and then decreases monotonically at higher concentrations, which indicates concentration quenching by energy transfer between two Sm^{3+} ions.

For LSB:Tb, the STE emission decreases with increase in the Tb^{3+} concentration (1-40 at.%), as shown in Fig. 3(c). An increase in the $^5D_4\rightarrow{}^7F_J$ transition of Tb^{3+} accompanies the decrease of the STE emission, which also indicates efficient energy transfer from the STE to Tb^{3+} ions. The two decay times of the intrinsic emissions, II (85 ns) and III (2.5 μs), become shorter in the Tb^{3+}-doped samples, which is consistent with the decrease in the time-averaged STE emission intensity with increasing Tb^{3+} concentration.

The Sm^{3+}/STE or Tb^{3+}/STE ratios gradually increase in intensity with temperatures from 7.8 to 293 K, which suggests that the energy transfer from the STE to Sm^{3+} or Tb^{3+} is thermally activated.

Fig. 1(a). Fig. 1(b).

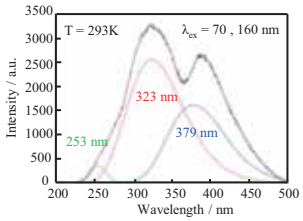

Fig. 2.

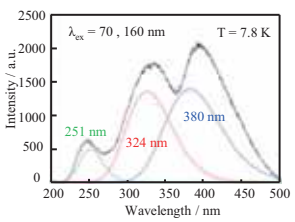

Fig. 3(a)

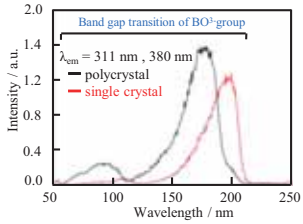

Fig. 3(b).

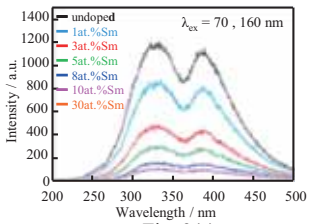

Fig. 3(c)

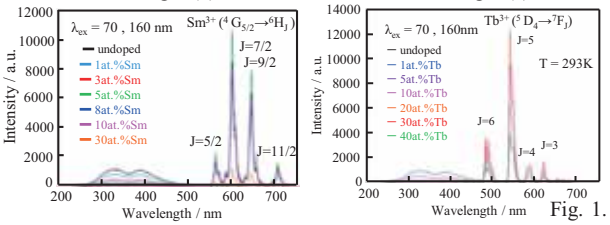

Fig. 1.

Emission spectra observed in undoped LSB excited at 70 nm and 160 nm at 293 K (a) and 7.8 K (b).

Fig. 2. Excitation spectra of undoped LSB poly- and single-crystal.

Fig. 3. Emission spectra of undoped LSB (a), LSB:Sm (b) and LSB:Tb excited at 70 nm and 160 nm.

[1] S.P. Feofilov *et al*., Phys.Rev.B. **74** (2006) 085101.

[2] S.P. Feofilov *et al*., J. Lumin. **125** (2007) 80.

[3] N. Kodama *et al*., *Abstract of 15th Int. Conf. on Defects in Insulating Materials* (2010) A90.

[4] K.Kan'no *et al*., Pure & Appl. Chem. **69** (1997) 1227.

Effect of Ion Implantation on the Crystallinity of $YAlO_3$ Single Crystal

Y. Horii, T. Morimoto and Y. Ohki
Waseda University, 3-4-1 Ohkubo, Shinjuku-ku, Tokyo 169-8555, Japan

Yttrium aluminate ($YAlO_3$) is a promising candidate for a gate insulator in advanced MOS devices. However, ion implantation, which is usually required after the deposition of a gate insulator, would cause damage to the gate insulator. Therefore, the effects induced by implantation of ions were examined by measuring optical absorption, photo-luminescence (PL) and X-ray diffraction (XRD) spectra.

The samples examined are commercially available $YAlO_3$ (100) single crystals in the shape of a plate with a thickness of 0.5 mm. Positive phosphorus (P^+) or boron (B^+) ions were implanted to the samples at a fluence of 1.0×10^{15} cm^{-2}. Before and after the ion implantation, optical absorption, in-plane XRD and PL were measured.

Optical absorption increases significantly at energies slightly lower than the gap energy as shown in Fig. 1. The XRD peak shown in Fig. 2 shifts after the implantation of P^+ and B^+ ions. Furthermore, its peak height becomes smaller. Figure 3 shows PL spectra induced by 6.4, 7.7 and 8.2 eV photons, where curve A represents PL spectra observed before ion implantation, while curves B and C represent those observed after the implantation of P^+ and B^+ ions, respectively. Among several photoluminescence bands observable in $YAlO_3$, two bands due to Cr^{3+} at around 1.70 eV induced by 6.4 eV photons [1], another one due to self-trapped exciton at 4.2 eV induced by 7.7 eV photons [2], and another one due to an antisite defect at 5.5 eV induced by 8.2 eV photons [3] become smaller or disappear by the ion implantation. These three PLs appear only when the sample is crystalline [1, 3, 4]. All these facts indicate that the appearance of localized electronic states in the band gap and the degradation of crystallinity are induced by the ion implantation.

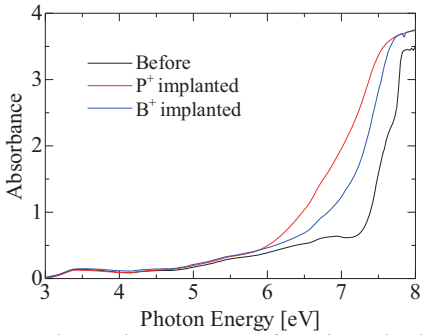

Fig. 1. Absorption spectra of $YAlO_3$ single crystals implanted with P^+ or B^+ ions.

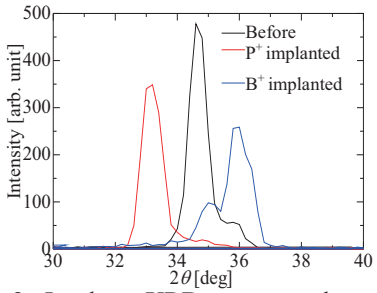

Fig. 2. In-plane XRD patterns observed before and after the implantation of P^+ or B^+ ions.

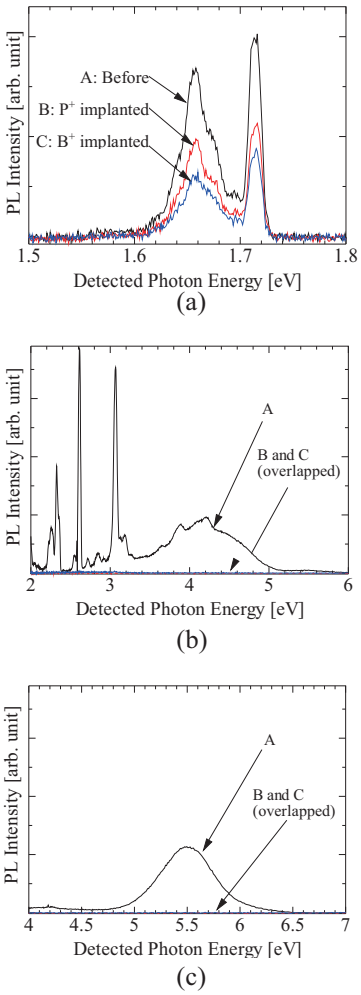

Fig. 3. PL spectra observed before and after P^+ or B^+ ion implantation, induced by 6.4 eV (a), 7.7 eV (b) and 8.2 eV (c) photons.

[1] E. Hirata *et al.*, Jpn. J. Appl. Phys. **49** (2010) 091102.
[2] Ch. Lushchik *et al.*, J. Phys. Condens. Matter **6** (1994) 11177.
[3] Y. V. Zorenko *et al.*, Opt. Spectrosc. **96** (2004) 536.
[4] M. Murakami *et al.*, J. Appl. Phys. Lett. **78** (2001) 2664.

BL3B

Optical Spectroscopy of Eu^{3+} in GaN Codoped with Mg and Eu

M. Yamaga, S. Tsuda and K. Takagi

Department of Mathematical and Design Engineering, Gifu University,Gifu 501-1193, Japan

Europium doped GaN is a candidate of red light-emitting diodes (red LEDs). Recent optical spectroscopy of Eu^{3+} in GaN(Mg) has revealed the electronic structure of Eu^{3+} associated with defects and temperature-dependence hysteresis of the Eu^{3+} luminescence [1]. However, the quantum efficiency of the Eu^{3+} luminescence was less than 1 %. In order to improve the quantum efficiency, it is very important to examine the relaxation process from the band-to-band excitation to the Eu^{3+} excited state.

GaN films, grown by hydride vapor phase epitaxy (HVPE) on (0001) sapphire substrates and doped with Mg (p-type) were implanted with 300 keV Eu ions. The GaN(Mg):Eu sample was supplied by Prof. K. P. O'Donnell at University of Strathclyde, UK.

Figure 1 shows the absorption spectrum of GaN(Mg):Eu at 300 K. The sharp step around 360 nm is corresponding to the band-edge energy of GaN. The interference fringes due to the thin film structure were observed in the spectrum.

The band-to-band excitation below 360 nm produces fairly strong Eu^{3+} luminescence lines around 620 nm, and three broad bands with peaks at 440, 540 and 600 nm as shown in Fig. 2. The Eu^{3+} luminescence lines decrease drastically beyond 360 nm and the two broad bands at 440 and 540 nm appeared clearly. These broad bands may be assigned to localized centers, for example, donors, acceptors or defects.

Relaxation to Eu^{3+} and emitting processes of Eu^{3+} are strongly associated with the rise and falling components of the decay curves of the Eu^{3+} luminescence, respectively. The decay curve of the Eu^{3+} luminescence in GaN:Eu can fit a single exponential function with the decay time of 0.23 ms [2]. However, the decay curve from GaN(Mg):Eu does not fit to a single exponential, but multi-exponential, at least three components. Otherwise, the decay curve fits to a sum of a single exponential function and power function of t^{n} (n=-1), assuming that there are two different relaxation processes to Eu^{3+}; one is rapid relaxation from band-to-band excitation immediately to the Eu^{3+} excited states; the other is relaxation to Eu^{3+} via donor-acceptor recombination process. Namely, the long decay time (larger than 2 ms) of Eu^{3+} may be due to fairly long feeding time. The possible model is shallowly trapped centers, for example, donors or acceptors trapping weakly electrons or holes, respectively. These bands with the double peaks at 440 nm and 540 nm in Fig. 2 may be associated with splitting of the acceptor bands consisting of Mg and N wavefunctions.

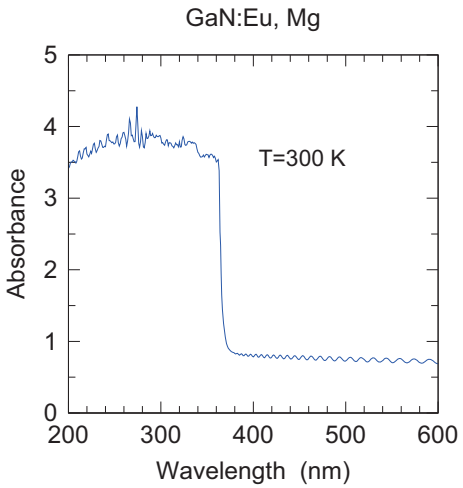

Fig. 1. The absorption spectrum of GaN(Mg):Eu.

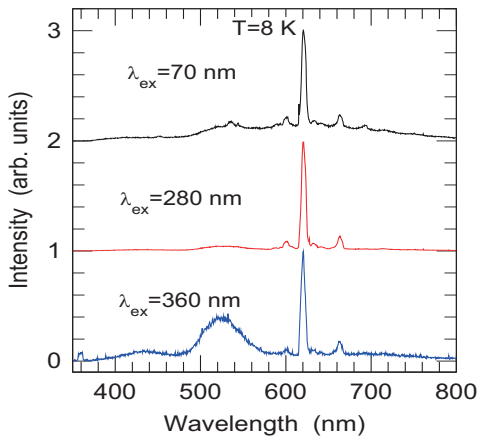

Fig. 2. Photoluminescence of Eu^{3+} in GaN(Mg):Eu excited with various wavelengths in the band-to-band transitions.

[1] K. P. O'Donnell, P. R. Edwards, R. W. Martin, K. Lorenz, V. Darakchieva, A. Alves and M. Bockowski, to be published (2013).
[2] I. S. Roqan, K. P. O'Donnell, R. W. Martin, P. R. Edwards, S. F. Song, A. Alves and M. Bockowski, Phys. Rev. B **81** (2010) 085209.

BL3B

Photoluminescence due to Intraionic 4*f*-4*f* Transitions of Gd^{3+} Ions in $Gd_3(Al,Ga)_5O_{12}$ Single Crystals

S. Ishii[1], M. Kitaura[1] K. Kamada[2], A. Ohnishi[1] and M. Sasaki[1]

[1]*Dept. of Physics, Faculty of Science, Yamagata University, 1-4-12 Kojirakawa, Yamagata 990-8560, Japan*

[2]*Materials laboratory of Furukawa Co. Ltd, 1-25-13 Kannondai, Tsukuba 305-0856, Japan*

Resonant energy transfer between impurity ions has been studied in the viewpoint of fundamentals and applications in inorganic phosphor materials [1]. The control of this process is one of conventional methods to enhance the luminescence yield in the development of phosphor materials. The main work is to hunt for better combinations of donor and acceptor ions on the basis of an overlap of absorption and luminescence spectra. The pair of Ce^{3+} and Gd^{3+} ions is known to be one of such combinations. In most ionic crystals, the absorption due to 4*f*-5*d* transitions of Ce^{3+} ions and the emission due to 4*f*-4*f* transitions of Gd^{3+} ions are located in the near ultraviolet range [2]. Since they have a strong overlap with each other, resonant energy transfer from Gd^{3+} to Ce^{3+} ions are possible in crystals including them.

$Gd_3Ga_3Al_2O_{12}$ (GAGG) belongs to the cubic system with garnet structure. Ce^{3+} doped GAGG (Ce:GAGG) attracts much attention as an inorganic scintillator for the detection of x- and γ–rays, because it has scintillation properties superior to other optical crystals [3]. As mentioned above, since the Ce:GAGG crystal contains Gd^{3+} and Ce^{3+} ions, there is the possibility that host sensitization of the Ce^{3+} 5*d*-4*f* emission occurs by the energy transfer from Gd^{3+} to Ce^{3+} ions. An investigation of the host sensitization process is of great significance for the realization of higher luminescence yield and shorter decay time, so it is worthwhile to investigate photoluminescence (PL) properties of GAGG crystals with vacuum ultraviolet (VUV) photons. In the present study, we have measured PL and PL-excitation (PLE) spectra of GAGG crystals with use of synchrotron radiation. Experiment was carried out at the BL3B beam line of UVSOR. Here, we report a part of results in our experiment.

Figure 1 shows the absorption spectrum of GAGG at 6K. Narrow peaks are observed around 4 –5 eV. Similar peaks have been observed for Gd^{3+} activated phosphors [2]. We thus assign them to 4*f*-4*f* transitions of Gd^{3+} ions. The strong absorption occurs at 5.96 eV. This corresponds to the fundamental absorption edge of GAGG.

Figure 2 shows PL and PLE spectra of a GAGG crystal. The PL spectrum was obtained at 6 K under excitation at 6.52 eV. A sharp peak appears at 3.92 eV in the PL spectrum. The PLE spectrum for the 3.92 eV peak exhibits narrow peaks, due to 4*f*-4*f* transitions of Gd^{3+} ions, around 4 – 5 eV. The 3.92 eV PL peak is also assigned to 4*f*-4*f* transitions of Gd^{3+} ions, because this peak is efficiently excited in the same position as narrow peaks in Fig. 1. As the photon energy is increased, the excitation for the 3.92 eV peak occurs at the fundamental absorption edge at 5.96 eV again, and it continues for the high-energy side above 5.96 eV. The intensity of the 3.92 eV peak is gradually increased around 20 eV, and reaches twice at 30 eV. This is interpreted as an appearance of the multiplication of electron-hole pairs in GAGG.

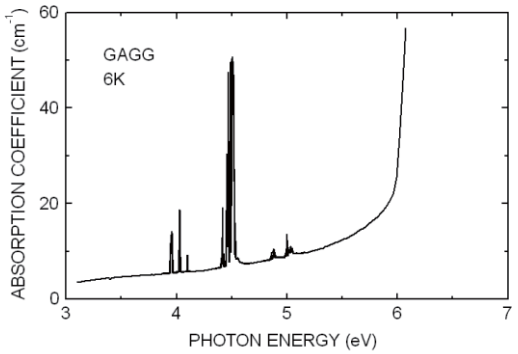

Fig. 1. Absorption spectra of a GAGG single crystal observed at 6 K.

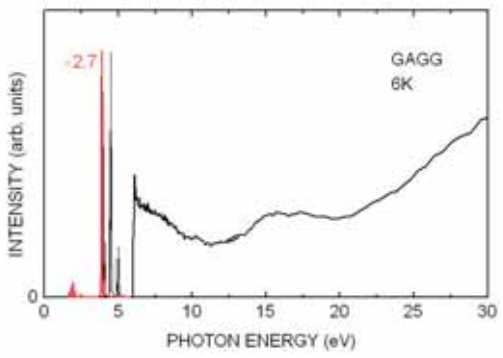

Fig. 2. Emission (red line) and excitation (black line) spectra of a GAGG single crystal observed at 6 K. The emission spectrum was observed under excitation at 6.52 eV. The excitation spectrum was measured for the 3.92 eV emission peak.

[1] D. L. Dexter, J. Chem. Phys. **21** (1953) 836.
[2] T. Kano, *Phosphor Handbook*, CRC Press (Boca Raton) 2nd ed., Chap.3, Sect.3 .
[3] K. Kamada *et al*., J. Cryst. Growth **352** (2012) 88.

BL4B

Nitrogen Doped TiO_2 Photocatalyst Prepared by Low Energy N^+ Implantation

T. Yoshida[1], E. Kuda[2] and H.Yoshida[2]

[1]*EcoTopia Science Institute, Nagoya University, Nagoya 464-8603, Japan*

[2]*Department of Applied Chemistry, Graduate School of Engineering, Nagoya University, Nagoya 464-8603, Japan*

Photocatalytic reactions at the surface of titanium dioxide (TiO_2) under UV light irradiation have been attracting much attention in view of their practical applications to environmental cleaning such as self cleaning of tiles, glasses, and windows. Asahi *et al.* reported that the substitutional doping of N into TiO_2 contributes to band gap narrowing to provide visible-light response [1].

In our previous study, we prepared visible-light response TiO_2 photocatalysts by the implantation of 50 keV N^+ ions [2]. We found that the photocatalytic active nitrogen species, i.e., nitrogen substituting for the O sites in TiO_2, are preferentially formed in the samples implanted with a low N^+ fluence (< 3 x 10^{21} m^{-2}). In the samples prepared with a higher N^+ fluence, the inactive N-O species generated to reduce photocatalytic activity. In the present study, a low energy, 5 keV N^+ implantation was performed in order to inject nitrogen atoms near the surface of TiO_2.

The samples used in this study were TiO_2 (1 0 0) single crystals (5 x 5 x 0.5 mm^3). Mass analyzed 10 keV N_2^+ (5 keV N^+) ions were injected into the samples at room temperature, perpendicular to the sample surface. As calculated by a Monte Carlo simulation using SRIM code (Fig. 1), the implanted nitrogen distributes up to ca. 25 nm, peaking around 10 nm in depth from the surface, and they would increase monotonously with N^+ fluence. Thus, the 5keV N^+ implantation enables to inject nitrogen atoms in the shallower region compared with the 50 keV N^+ implantation in our previous study.

N K-edge XANES spectra of the samples were measured at the BL-4B. Data were recorded at room temperature in total electron yield mode.

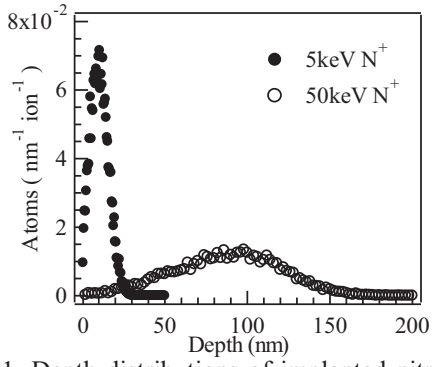

Fig. 1. Depth distributions of implanted nitrogen per incident N^+ ion calculated by SRIM code for 5 and 50 keV N^+ implantations.

Figure 2 shows N K-edge XANES spectra of the N^+-implanted TiO_2 and TiN samples. Common XANES features in (b) and (d) suggest that N in the sample implanted by 3 x 10^{21} m^{-2} (TiO_2-N(3)) is in a chemical environment similar to that in TiN. Careful observation led us to notice that two peaks around 400 eV for the catalyst sample shift to lower energy side than those for the TiN sample, which was well reproduced by the theoretical prediction using FEFF code when N occupies one of the O sites of TiO_2.

On the other hand, the XANES spectra of the sample implanted by 1 x 10^{21} m^{-2} (TiO_2-N(1)) and that implanted by 3 x 10^{21} m^{-2} followed by heating at 573 K (TiO_2-N(3)-H) showed a distinct single peak around 401 eV. This peak could be empirically attributed to formation of the species such as NO bonds near the surface [3], and which also indicates that the inactive N-O species dominates in TiO_2-N(1) and the active nitrogen formed in TiO_2-N(3) changed to the inactive N-O species by oxidation at 573 K. These results are in conflict with our previous study, in which the photocatalytically active nitrogen was preferentially produced by 50keV N^+ implantation with the lower nitrogen concentration.

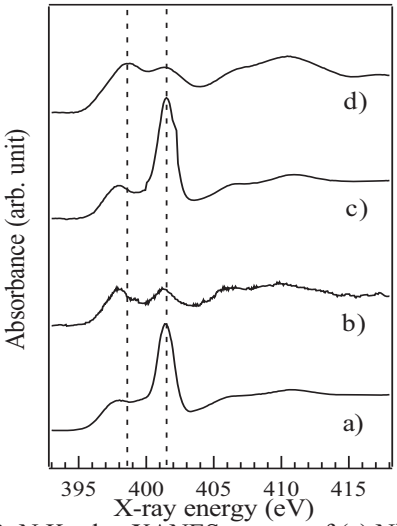

Fig. 2. N K-edge XANES spectra of (a) N^+-implanted at 1 x 10^{21} m^{-2}, (b) N^+-implanted at 3 x 10^{21} m^{-2}, (c) N^+-implanted at 3 x 10^{21} m^{-2} followed by heating at 573 K for 2 h, and (d) TiN.

[1] R Asahi *et al.,* Science **293** (2001) 269.
[2] T. Yoshida *et al.,* Mater. Trans. **48** (2007) 2580.
[3] J-H. Wang *et al.,* Anal. Chim. Acta, **476** (2003) 93.

BL4B

Surface-Structure Change in Lithium-Ion Battery Using Anti-Fluorite Type Positive Electrode

T. Okumura, M. Shikano and H. Kobayashi

National Institute of Advanced Industrial Science and Technology (AIST), Ikeda, Osaka 563-8577, Japan

Fe-based materials as positive electrodes of lithium-ion batteries have been paid much attention to due to their advantages of being low cost and environmentally benign. For example, $LiFePO_4$ is used as the positive electrode material of commercial lithium-ion batteries in spite of relatively lower capacity. To improve battery performance, the positive electrode materials of high capacity are required. Defect anti-fluorite-type structure Li_5FeO_4 is one of the candidate because its theoretical capacity reaches ~694 mAh g^{-1} (four Li in a formula unit) [1, 2]. In previous work, the relatively rechargeable capacity of Li_5FeO_4 could be obtained after first charging until two Li per Li_5FeO_4 formula unit [1]. However, the changes in electronic and crystal structure of Li_5FeO_4 during the electrochemical reaction have not been clarified yet. Recently, we have analyzed the structural changes of Li_5FeO_4 during charging process using XRD, hard-XAFS and ^{7}Li MAS NMR. In this study, the surface-structure change during electrochemical reaction was analyzed by O *K*-edge XAFS spectra using total-electron-yield (TEY) mode.

Li_5FeO_4 was synthesized by solid-state reaction. The positive electrodes were made from a mixture containing 60 wt% Li_5FeO_4, 32 wt% acetylene black and 8 wt% polytetrafluoroethylene, which were casted and pressed on nickel mesh. Coin cells were assembled using metallic lithium foil as a negative electrode. A 1 mol dm^{-3} ethylene carbonate/dimethyl carbonate solution of $LiPF_6$ was used as electrolyte. Electrochemical test was carried out at a constant current density of 1/30 C. For measuring XAFS spectra, samples (#1~5) were obtained from the cells after charging or discharging, as shown in Fig. 1.

The O *K*-edge spectra were shown in Fig. 2+. 3*d*-transition metal (*TM*) oxides generally have the two peaks around 532-538 eV since O 2*p* orbital hybridized with *TM* 3*d* t_{2g} and e_g as shown in the spectrum of Fe_2O_3. However, this specific shape could not be observed in the all samples in this study (#1~5). This result indicates that the surface of the samples is covered with another phase containing lithium salts, and iron oxide phase could not be detected by TEY mode. To identify the surface phase, the spectra of various lithium salts were measured as partially shown in Fig. 2. The spectrum of pristine sample (#1) is similar to that of Li_2O, that is, the surface of #1 would be covered with Li_2O since the lattice parameters of anti-fluorite-type structure Li_2O is close to those of Li_5FeO_4. The shapes of the spectra around 535-538 eV were changed during charging battery (#1 to #4). Thus, the surface Li_2O also reacts as well as the oxidation of internal Li_5FeO_4 phase. For example, Li_2O_2 is one of the candidates of product compounds. After that, the Li_2O re-formed after discharging battery (#5). Thus, the electrochemical reaction of the surface Li_2O phase would also contributed on the charge / discharge properties in the battery using anti-fluorite Li_5FeO_4 positive electrode.

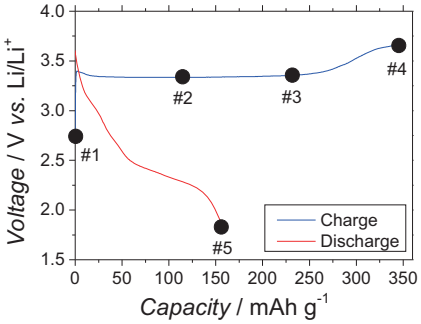

Fig. 1. First cycle of lithium-metal half cell using Li_5FeO_4 positive electrode. Circles indicate the samples measured XANES spectra.

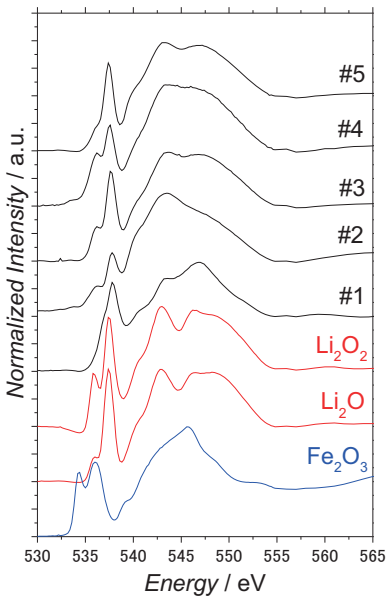

Fig. 2. O *K*-edge XANES spectra measured by total-electron-yield mode.

[1] A. Hirano *et al.,* Solid State Ionics **176** (2005) 2777.
[2] C.S. Johnson *et al.,* Chem. Mater **22** (2010) 1263.

BL5U

Ultrahigh-Resolution Direct Observation of Mini-bands Formed in InGaAs/AlGaAs Superlattice

D. Shimura[1], F. Ichihashi[1], K. Nishitani[1], S. Harada[1], M. Kuwahara[2], T. Ito[1], M. Matsunami[3], S. Kimura[3], M. Tagawa[1] and T. Ujihara[1]

[1]*Department of Materials Science and Engineering, Nagoya University, Nagoya 464-8603, Japan*
[2]*Department of Applied Physics, Nagoya University, Nagoya 464-8603, Japan*
[3]*UVSOR Facility, Institute for Molecular Science, Okazaki 444-8585, Japan*

Intermediate-band solar cells have attracted great attention for their potential to achieve 74.6 % efficiency over the Shockley-Queisser limit of a single gap solar cell [1-3]. The concept of the intermediate-band solar cell is to increase photocurrent by using electrons excited to a conduction band via the intermediate-bands. Mini-bands formed in superlattice structures are often utilized for the formation of the intermediate-bands. Indeed, recently, it has been demonstrated that quantum-well superlattice solar cells induced two step photon absorption and photocurrent generation at room temperature [4]. In addition, these reports indicated that the transport of the carriers in the mini-bands was essential in order to the photocurrent generation based on two step absorption. Therefore it is very important to figure out the mini-band structures which influence the transport properties and the conversion efficiency. In this study, we directly observed the dispersions of mini-bands formed in InGaAs/AlGaAs quantum-well superlattice by angle-resolved photoemission spectroscopy (ARPES) with synchrotron radiation.

The structure of the specimen is shown in Fig. 1. The superlattice was grown by a low-pressure metalorganic vapor phase epitaxy. On the evaluation of the mini-band structure, normal-emission and in-plane ARPES measurements in the vacuum-ultraviolet region were performed at BL5U of the UVSOR-III storage ring. The measurements were carried out at 10 K under the ultrahigh vacuum atmosphere (less than 1×10^{-8} Pa).

The ARPES intensity mapping image of the *X*-valley of InGaAs which was originated from the surface of the superlattice specimen is shown in Fig. 2. The zero energy indicates the valence-band maximum and the zero wave vector indicates the *X*-valley. The valence band of InGaAs and As 3*d* core level-derived peaks were observed. In addition, it was noticed that the peaks which were not existed in the InGaAs bulk were observed ranging from -2.0 to 0 eV of energy. The yellow circles indicate the mini-band-derived peaks of the second order differential, which indicate the mini-band structures formed in the superlattice structure. These peaks were good consistent with the theoretical values calculated by Kronig-Penney model, especially the heavy hole mini-bands.

By ARPES measurement at high resolution, we can experimentally evaluate the mini-band structures.

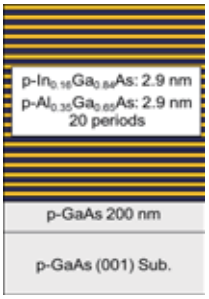

Fig. 1. Details of the structures of the specimen.

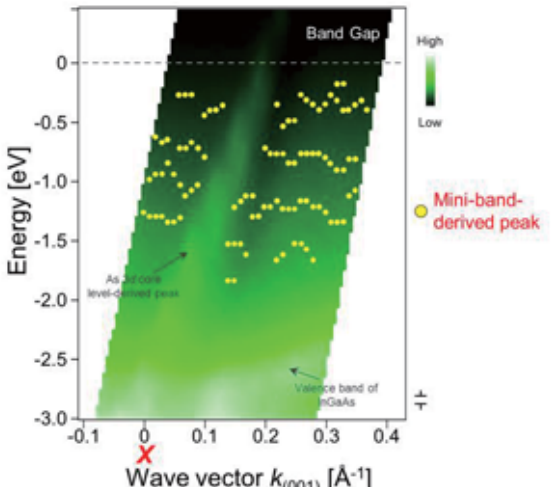

Fig. 2. The ARPES intensity mapping image of InGaAs/AlGaAs superlattice. The yellow circles indicate the mini-band-derived peaks of the second order differential.

[1] A. Luque and A. Martí, Phys. Rev. Lett. **78** (1997) 5014.
[2] T. Nozawa and Y. Arakawa, Appl. Phys. Lett. **98** (2011) 171108.
[3] W. Shockley and H. J. Queisser, J. Appl. Phys. **32** (1961) 510.
[4] M. Sugiyama, Y. Wang, K. Watanabe, T. Morioka, Y. Okada and Y. Nakano, IEEE J. Photovoltaics **2** (2012) 298.

BL5B

Characterization of Amorphous Chalcogenide Films by Vacuum Ultraviolet Absorption Spectroscopy

K. Hayashi

Department of Electrical and Electronic Engineering, Gifu University, Gifu 501-1193, Japan

Amorphous semiconductor materials are very expected as a potential material for optoelectronic devices because these materials are very sensitive to the light and show a variety of photoinduced phenomena [1-3]. For the device application, it is necessary to sufficiently understand the physical property of these materials. Although a large number of studies have been done on the photoinduced phenomena of these materials, little is known about the details of these mechanisms. These phenomena were studied by exciting outer core electrons with the irradiation of light with the energy corresponding to the optical bandgap or sub-bandgap. The interest has been attracted for the change of the optical properties in the energy region of the visible light. We are interesting for the changes of the optical properties in the higher energy region. To obtain a wide knowledge of the photoinduced phenomena, it is necessary to investigate to the photoinduced effects on wide energy region. In previous reports, we reported the photoinduced change at the VUV reflection and total photoelectron yield spectra of the amorphous chalcogenide thin films induced by bandgap light. Recently, we became able to measure directly the VUV absorption spectra of amorphous thin films [4]. In this paper we report results on the study of the difference of the structure between the as-deposited and well-annealed films by the VUV absorption spectroscopy.

Samples used for the measurement of the VUV absorption spectrum were amorphous chalcogenide (a-As_2S_3 and a-As_2Se_3) semiconductor thin films prepared onto aluminum thin films by conventional evaporation technique. Typical thickness of the samples and the aluminum films were around 180nm and 100nm respectively. The aluminum film was also used in order to eliminate the higher order light from the monochromator in the VUV region. The measurements were carried out at room temperature at the BL5B beam line of the UVSOR facility of the Institute for Molecular Science. And the spectrum was measured by using the silicon photodiode as a detector. A pinhole of 1.5mm in a diameter was inserted between the monochromator and sample to remove stray light. The intensity of the VUV light was monitored by measuring the TPEY of a gold mesh. The positions of the core levels for the samples were calibrated by referencing to the 2p core level absorption peak of the aluminum film.

Figure 1 shows VUV absorption spectra of As 3d core level for the as-deposited and the well-annealed amorphous chalcogenide films. As shown in the figure, the As 3d core level absorption peaks of the as-deposited film show significant differences in shapes and positions in comparison with those obtained for the well-annealed film. It can explain the difference by the reports [5] that many dangling bonds and homo bonds (As-As and S-S bonds etc.) exist in the as-deposited amorphous films. In the next step, the structural changes by the irradiation of the bandgap light will be investigated by the VUV absorption spectroscopy.

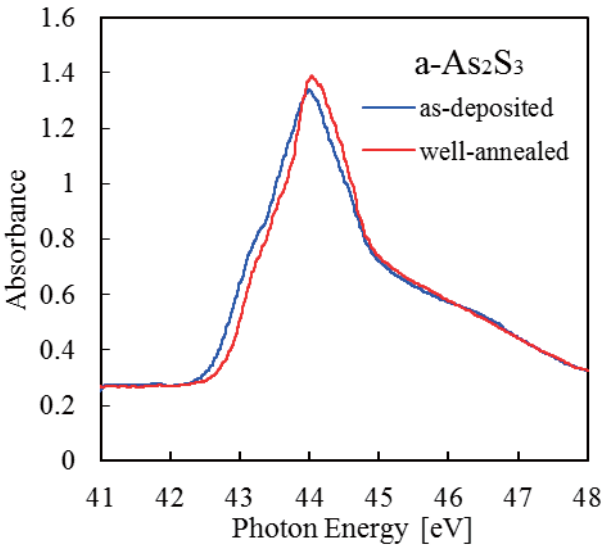

Fig. 1. VUV absorption spectra of As 3d core level for as-deposited and well-annealed amorphous chalcogenide films.

[1] Ke. Tanaka, Rev. Solid State Sci. **4** (1990) 641.
[2] K. Shimakawa, A.Kolobov, and S. R. Elliott, Adv. Phys. **44** (1995) 475.
[3] Ke. Tanaka, Encyclopedia of Nanoscience and Nanotechnology, **7** (2004) 629.
[4] K. Hayashi, UVSOR Activity Report **34** (2007) 79.
[5] Ka. Tanaka, Researches of the Electrical Laboratory, **779** (1977) 35.

BL6U

Highly Ordered Multilayer Films of Fragile Bio-Molecules - The Band Dispersion in Adenosine and Guanosine Assemblies

R. Friedlein[1], S. Z. N. Demon[1], H. Yamane[2] and N. Kosugi[2]

[1]*School of Materials Science, Japan Advanced Institute of Science and Technology, Nomi, Ishikawa 923-1292, Japan*

[2]*Dept. of Photo-Molecular Science, Institute for Molecular Science, Okazaki 444-8585, Japan*

Guanosine and adenosine are purine nucleosides that are composed of guanine or adenine units, respectively, attached to a ribose sugar. Their molecular structure is depicted in Figure 1 a and b, respectively. As the basic units of RNA and DNA, as well as in the case of adenosine-triphosphate (ATP) as the primary energy source for most bio-molecular processes, they are in the center of life itself.

Since these fragile bio-molecules decompose at elevated temperatures, however, it has been intrinsically difficult to investigate the electronic properties of their assemblies using surface science techniques. In the present study, thin multilayer films of adenosine, guanosine as well as of the Na salt of guanosine triphosphate (Fig. 1c) have been processed at about 100 °C onto graphite (0001) surfaces by spray deposition from solution inside a home-based ultra-high vacuum system. Films were then exposed *in situ* to water vapor before being transferred on air to the experimental set-up at BL 6U.

Photon-energy dependent photoelectron spectra of about an about 2-4 nm thick adenosine film were obtained at normal emission with photon energies in between 43 and 130 eV. As shown in Fig. 1d), a pronounced feature related to the highest occupied molecular orbital (HOMO), centered at a binding energy of about 2.8 eV, is composed of at least two bands, denoted “A” and “B”. While the dispersion of the one at lower energy, “A”, can be traced over several periods, “B” appears to be non-dispersing. As shown recently for guanine and adenine thin films [1, 2], the presence of dispersing π electronic states indicates the formation of homeotropically aligned, highly-ordered columnar assemblies. A more precise evaluation of the band dispersion of “A” with a one-dimensional tight-binding fit reveals the band width of 384 ± 20 meV and the length of the repeat unit of 6.78 ± 0.03 Å which is consistent with two inequivalent molecules per unit cell and the size of the overlap integral of 96 ± 5 meV. Note that the stacking is distinguishably different from that in adenine assemblies with its four molecules per unit cell [2] and also from DNA and RNA spiral configurations.

Guanosine triphosphate within films of its Na salt and guanosine have been found to form thin films which are structurally and electronically similar to those of adenosine. Our results show that the presence of water molecules within the crystal does not prevent the formation of extended electronic states as required for a band-like charge transport along quasi-one-dimensional assemblies.

This work was supported by the Joint Studies Program (No. 608, 2012-2013) of the Institute for Molecular Science.

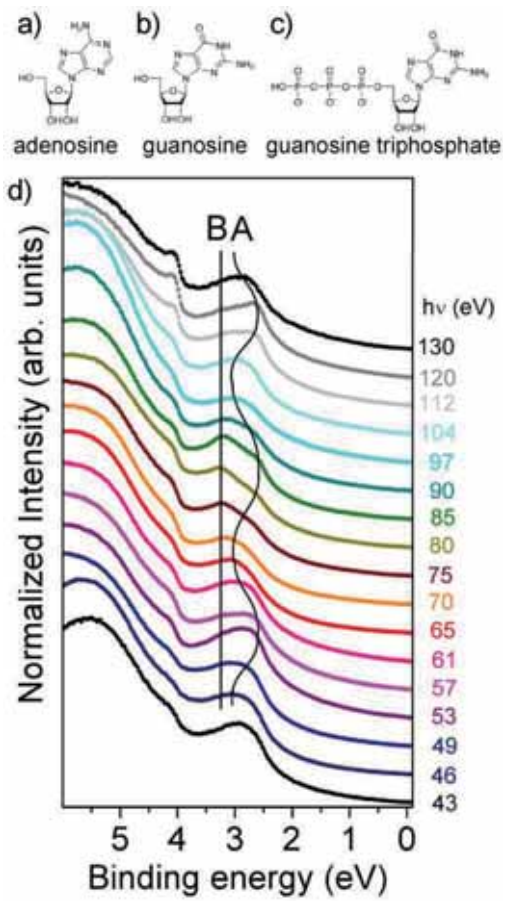

Fig. 1. Photon-energy dependent photoelectron valence band spectra of the hydrated adenosine multilayer films. “A” and “B” denote features related to HOMO-derived electronic states.

[1] R. Friedlein, Y. Wang, A. Fleurence, F. Bussolotti, Y. Ogata and Y. Yamada-Takamura, J. Am. Chem. Soc. **132** (2010) 12808.

[2] Y. Wang, A. Fleurence, Y. Yamada-Takamura and R. Friedlein, Chem. Commun. **47** (2011) 12349.

BL6B

Far-Infrared Reflective Study of Alkali Niobate Ceramics

T. Nishi, K. Tsuchida, K. Kato, N. Kato, M. Watanabe and K. Kakimoto
Graduate School of Engineering, Nagoya Institute of Technology, Nagoya 466-8555, Japan

Alkali niobate ceramics are one of the promising candidates for lead-free piezoelectric materials. Especially, Li-doped (Na,K)NbO_3 (LNKN) solid solution shows excellent piezoelectric properties. Although it has been expected that the distortion of lattice structure due to the small ionic diameter of substited-Li ion would contribute to the good ferroelectric properties, the particular reason for this is still unclear. In our previous work, we evaluated the local lattice structure of alkali niobate ceramics using FT-IR analysis. The present work reports the spectroscopic characterization of LNKN ceramics using infrared (IR) technique.

The $Li_x(Na_{0.5}K_{0.5})_{1-x}NbO_3$ ceramic samples were produced by a solid-state reaction method. The surfaces of the LNKN ceramics were polished for IR reflectivity measurement. The reflectivity spectra were recorded in the range of 20 – 8000 cm^{-1} at room temperature using a synchrotron radiation source. The spectra were corrected by using a Michelson interferometer (Bruker, IFS66v). The IR reflectivity spectra were fitted by :

$$\varepsilon(\omega) = \varepsilon_\infty + \sum_n \omega^2_{pn} / \omega^2_{on} - \omega^2 - n\gamma_n\omega \qquad (1)$$

where, ε_∞ is the high-frequency dielectric constant, ω_p and ω_o are the plasma and longitudinal frequencies, and γ is the damping constant. The complex dielectric function is related to the reflectivity spectrum by the equation,

$$R = \left| \sqrt{\varepsilon(\omega)} - 1 / \sqrt{\varepsilon(\omega)} + 1 \right|^2 \qquad (2)$$

Figure 1 shows the reflectivity spectra of LNKN ceramics (x = 2 mol %) at room temperature. Figure 2 shows the complex permittivity (imaginary part) calculated from the fitting results (using eq. (1) and (2)). A weak phonon peak was observed around 100 cm^{-1}. This peak cannot be assigned with the only orthorhombic *Bmm*2 which represents NKN crystal structure (x = 0 mol %). Therefore, it can be found that Li substitution led to another phase in the NKN crystal structure. From XRD analysis, it has been obtained that LNKN ceramics possess the distorted monoclinic *Pm* phase. Therefore, this peak could be assigned with the mixed phase structure including monoclinic *Pm* phase. Figure 3 shows the phonon analysis results of LNKN ceramics by using FT-IR data. The phonon intensity around 100 cm^{-1} are increased with Li concentration. This result suggests that the proportion of *Pm* phase in LNKN ceramics increases with increasing the amount of Li content.

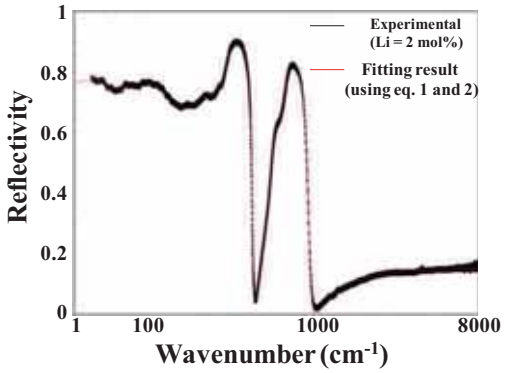

Fig. 1. Infrared reflectance spectra of $Li_{0.02}(Na_{0.5}K_{0.5})_{0.98}NbO_3$ ceramics at R.T. and red line represented fitting result using equations (1) and (2).

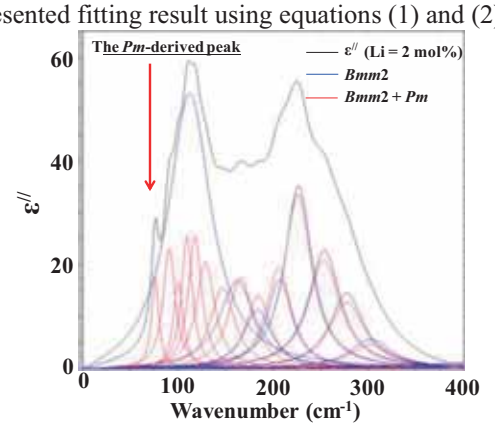

Fig. 2. Variation of imaginary part of permittivity with wavenumber for $Li_{0.02}(Na_{0.5}K_{0.5})_{0.98}NbO_3$ ceramic.

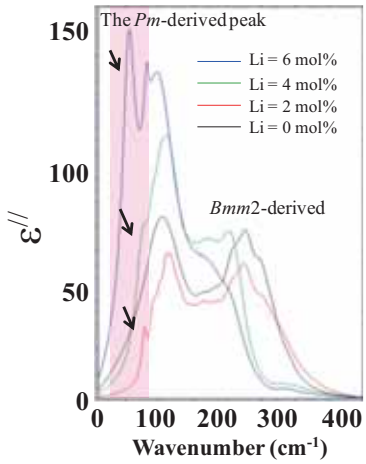

Fig. 3. Dependence of the imaginary part of permittivity on Li content in LNKN ceramics.

In the LNKN phonon spectra, more phonon modes are observed due to the existence of Li in the lattice. It is concluded that Li substation distorted the unit cell of the NKN ceramics and introduced the monoclinic *Pm* phase.

VUV Reflection Spectroscopy of Mg-Ni Alloy Thin Films

S. Sato, R. Matsushima, K. Hirasawa, M. Anzai and H. Matsumoto
School of Science & Technology, Meiji University, Kawasaki 214-8571, Japan

Magnesium nickel (Mg–Ni) alloy are well-known metallic alloys for hydrogen storage, and they exhibit switching mirror behavior from metal to transparent films. This behavior is due to the fact that the hydrides of the Mg–Ni alloys are transparent. The alternant hydrogenation and dehydrogenation reactions depend on their switching behavior. Therefore, the optical properties of these alloys are significantly changed by hydrogenation. However, there have been no reports about the optical properties of these Mg–Ni alloy materials in the vacuum ultraviolet (VUV) region. The transparent hydride forms of the Mg–Ni alloy films exhibit a large energy gap and fundamental absorption in the VUV region. VUV reflection spectroscopy is the one of the most important analysis methods for verifying the fundamental absorption properties of such transparent films [1, 2]. On the basis of VUV reflection spectroscopy, the refraction spectra of the hydride and dehydride forms of Mg–Ni alloy thin films prepared by the radio-frequency (RF) magnetron sputtering method were systematically investigated.

A switching Mg–Ni alloy film was prepared by the RF magnetron sputtering method according to Reference [3]. Metallic Mg (99.9%) and Ni plates (99.9%) were used as targets. The incident RF power was 100 W for Ni and 30–50 W for Mg. The sputtering was performed under an argon gas atmosphere at a total gas pressure of 0.8 Pa, and the argon flow was fixed at 20 sccm. The films were sputtered onto silica substrates at 100°C. The film thicknesses were approximately 100 nm. In addition, a 5-nm-thick palladium layer was deposited onto the films at room temperature. These films were maintained under a hydrogen (H_2) atmosphere for 24 h to prepare the hydride forms of the films.

Reflection spectra of the films were measured in the vacuum ultraviolet region up to 40 eV with a 3 m normal incidence monochromator (gratings: G1, G2, and G3) using the BL7B beamline at UVSOR-III. A silicon photodiode sensor was used as the detector for the reflected light.

Figure 1 shows the refraction spectra of Mg, Ni, and Mg-Ni alloy thin films before and after they were exposed to H_2. A change in the refraction spectra before and after H_2 exposure was observed only in the case of the Mg–Ni alloy thin film. The change in the spectra was more pronounced in the case of the Mg–Ni alloy thin film deposited with a Mg RF power of 40 W. As evident in the Fig. 1, no spectral changes were observed in the Mg and Ni films before and after the films were exposed to H_2. However, some strong peaks were observed in the region beyond 10 eV in the spectrum of the Mg–Ni alloy thin film after it was exposed to H_2. The positions of these peaks were 11, 14, 21, and 32 eV. The hydrogenation reaction of the Mg and Mg–Ni alloys is represented as follows [3]:

$$Mg_2Ni + 2H_2 \rightarrow Mg_2NiH_4$$
$$Mg + H_2 \rightarrow MgH_2$$

The peaks beyond 10 eV were assigned Mg_2NiH_4, which is the hydride form of the Mg–Ni alloy, because no changes were observed in the spectra of the Mg film. The transparent hydride of the Mg–Ni alloy film exhibited a large energy gap and fundamental absorption in the VUV region.

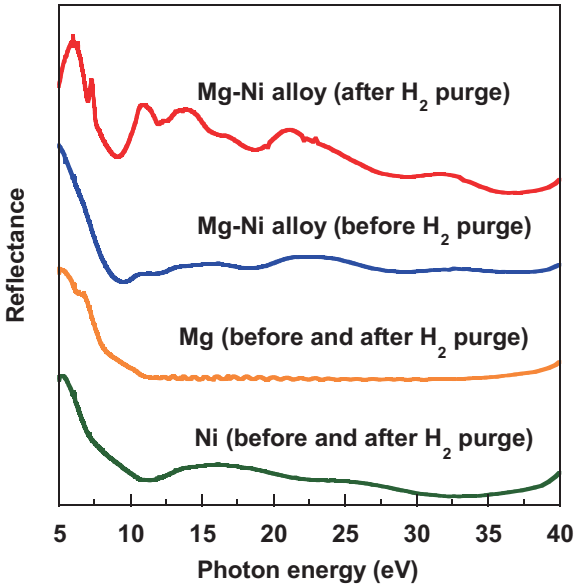

Fig. 1. Reflection spectra of Mg, Ni, and Mg-Ni alloy thin films before and after H_2 purge.

[1] K. Nakagawa *et al*., UVSOR Activity Report **32** (2005) 88.
[2] Y. Iwai *et al*., UVSOR Activity Report **35** (2008) 96.
[3] K. Yoshimura, J. Surf. Finish. Soc. Jpn **56** (2005) 882.

BL7B

Photoluminescence upon Vacuum Ultraviolet Excitation in Gd^{3+} Ion Doped Inorganic Materials

Y. Inaguma, R. Horiguchi, S. Sasaki and D. Mori

Department of Chemistry, Faculty of Science, Gakushuin University, Tokyo 171-8588, Japan

Recently phosphor materials emitting UV light upon vacuum ultra violet (VUV) excitation are desired as the substitutes of mercury lamp due to the toxicity of mercury. Among them, Gd^{3+} ion doped compounds are expected to be candidates of the UV phosphors since the f-f transition from ^6P_J to $^8S_{7/2}$ in Gd^{3+} corresponds to UV region [1-4]. The UV emission would be observed when the band gap energy of the host material is in the VUV region. In this study we then chose alkaline-earth phosphates with the band gap energy in the VUV region. Herein, we synthesized $A_3(PO_4)_2$:Gd^{3+}(A = Ca, Sr, Ba) and investigated the luminescence properties upon VUV excitation.

The polycrystalline samples of $A_3(PO_4)_2$:Gd^{3+}(A = Ca, Sr, Ba) were synthesized by a conventional solid state reaction at elevated temperature. The mixture of starting materials: alkaline-earth carbonate such as ACO_3 (A = Ca, Sr, Ba), $(NH_4)H_2PO_4$ and Gd_2O_3 or Gd nitrate solution were calcined at 1000°C in air. The calcined powder was pressed into pellets and sintered at 1000-1200°C in air. The phase identification for the samples was carried out by the powder X-ray diffraction (XRD) using a Rigaku RINT 2100 diffractometer with a Bragg Brentano geometry (graphite-monochromatized CuKα radiation). The emission and excitation spectra were recorded by a JASCO FP-6500 fluorometer upon the photo excitation using a Xe excimer lamp (λ = 172 nm) or in the beamline BL7B at the UVSOR facility.

The obtained samples were crystallized to be the hexagonal β-type form of tricalcium phosphates for A = Ca, and hexagonal form with a space group $R\bar{3}m$ for A = Sr and Ba. Figure 1 shows the emission spectra upon photo excitation of 172 nm for $A_3(PO_4)_2$: Gd^{3+} 5% (A = Ca, Sr, Ba) at room temperature. As seen in Fig.1, the UV emission peaks at 307 nm, 310 nm were observed for all compounds, which correspond to the f-f transitions, from $^6P_{5/2}$ to $^8S_{7/2}$, from $^6P_{7/2}$ to $^8S_{7/2}$ states of Gd^{3+}, respectively, and $Sr_3(PO_4)_2$: Gd^{3+} exhibited the highest emission intensity. Figure 2 shows the excitation spectrum emission-monitored at 310 nm for $Sr_3(PO_4)_2$: Gd^{3+} 1% at room temperature. Here, the excitation spectrum was corrected for the spectral distribution of excitation light source. In the excitation spectrum, the peaks around 142, 275, and 155 nm correspond to the f-f transitions from the ground state of $^8S_{7/2}$ to $^2Q_{23/2}$ state, $^8S_{7/2}$ to $^2Q_{23/2}$ of Gd^{3+}, and the host absorption band, i.e. the intra charge transfer of PO_4^{3-}[5, 6], respectively. While another peak at 130 nm has not been assigned at the present time.

Consequently, it was found that $A_3(PO_4)_2$: Gd^{3+} (A = Ca, Sr, Ba) exhibits UV emission corresponding to the f-f transition and they are candidates of UV phosphors upon VUV excitation.

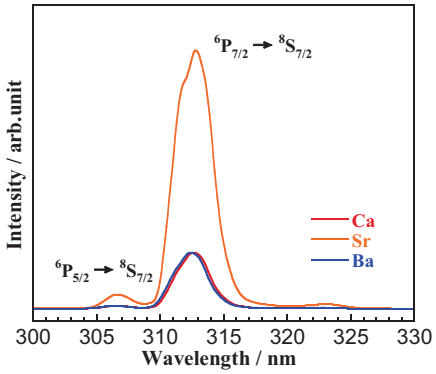

Fig. 1. Emission spectrum upon excitation of 172 nm for $A_3(PO_4)_2$:Gd^{3+}5% (A = Ca, Sr, Ba).

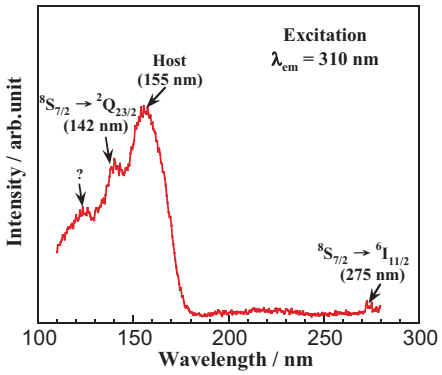

Fig. 2. Excitation spectrum monitored at 310 nm for $Sr_3(PO_4)_2$: Gd^{3+} 1%.

The authors thank Mr. M. Hasumoto, Prof. S. Kimura, and Prof. K. Fukui for their experimental supports and helpful advices.

[1] H. Yoshida, R. Yoshimatsu, S. Watanabe and K. Ogasawara, Jpn. J. Appl. Phys. Part .1 **45** (2006) 146.
[2] N. Yokosawa, G. Sato and E. Nakazawa, J. Electrochem. Soc. **150** (2003) H197.
[3] T. Hirai, H. Yshida, S. Sakuragi and N. Ohno, Jpn. J. Appl. Phys. Part .1 **46** (2007) 146.
[4] S. Okamoto, R. Uchino, K. Kobayashi and H. Yamamoto, J. Appl. Phys.,**106** (2009) 013522.
[5] E. Nakazawa and F. Shiga, J. Lumin. **15** (1977) 255.
[6] H. Liang, Y. Tao, J. Xu, H. He, H. Wu, W. Chen, S. Wang and S. Su, J. Solid State Chem. **177** (2004) 901.

Ascription of the Luminescent Components of Cs_2ZnCl_4 Single Crystal

N. Yahaba[1], M. Koshimizu[1], T. Yanagida[2], Y. Fujimoto[3], R. Haruki[4], F. Nishikido[5], S. Kishimoto[6] and K. Asai[1]

[1]*Department of Applied Chemistry, Graduate School of Engineering, Tohoku University, Sendai 980-8579, Japan*
[2] *Graduate School of Life Science and Systems Engineering, Kyushu Institute of Technology, Kitakyushu 808-0196, Japan*
[3]*Institute of Materials Research, Tohoku University, Sendai 980-8579, Japan*
[4]*Advanced Science Research Center, Japan Atomic Energy Agency, Tokai-mura 319-1195, Japan*
[5]*Molecular Imaging Center, National Institute for Radiological Sciences, Chiba 263-8555, Japan*
[6]*Institute of Materials Structure Science, High Energy Accelerator Research Ogranization, Tsukuba 305-0801, Japan*

Scintillation materials exhibiting short decay are highly required for detection of high-energy X-ray photons at high counting rate. Recently, we have found that Cs_2ZnCl_4 crystals have excellent scintillation characteristics. In this report, we present the luminescence and scintillation dynamics of Cs_2ZnCl_4.

Figure 1 shows the scintillation time profile excited with 50 keV X-ray. The profile was expressed as a sum of two exponential components. The fast and slow ones have lifetimes of 1.8 and 10 ns, respectively. The relative intensity of each component was different for different crystals. The relative intensity hardly depended on the raw materials. In contrast, the contribution of the slow component increased after annealing the crystal.

Figure 2 shows the luminescence spectra. Under excitation at 88 nm, two luminescence bands were observed at 290 and 380 nm. This result is quite similar to a previous report [1, 2], and these bands are ascribed to the Auger-free luminescence. In the case of excitation at 198 nm, luminescence was observed at 320 nm. In this case, the excitation photon energy was lower than the bandgap energy of Cs_2ZnCl_4, and thus the observed luminescence band was ascribed to defects or impurities.

Figure 3 shows the luminescence time profile under VUV excitation. The lifetime of the decay at 290 and 380 nm was estimated to be 2 ns, which is consistent with the fast component in the scintillation time profile. In contrast, the lifetime of the decay at 320 nm was estimated to be approximately 10 ns. These results indicate that the slow component is ascribed to defects would be eliminated by treating the crystal after growth.

[1] A. Ohnishi, M. Kitaura, T. Otomo and M. Sasaki, J. Phys. Soc. Jpn. **72** (2003) 2400.
[2] A. Ohnishi, M. Kitaura, M.Itoh and M. Sasaki, J. Phys. Soc. Jpn. **81** (2012) 114704.

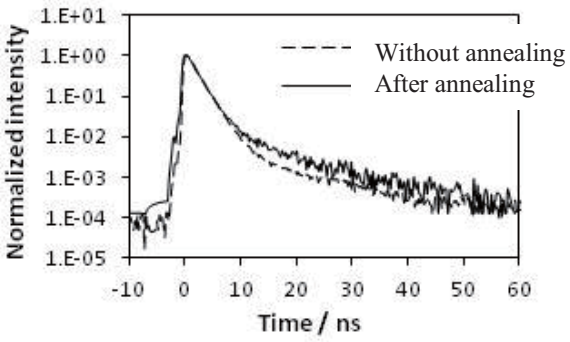

Fig. 1. Scintillation time profiles of Cs2ZnCl4 crystals before and after annealing.

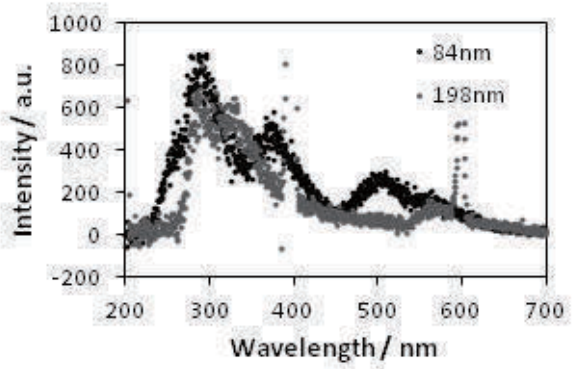

Fig. 2. Luminescence spectra of Cs_2ZnCl_4 under VUV excitation.

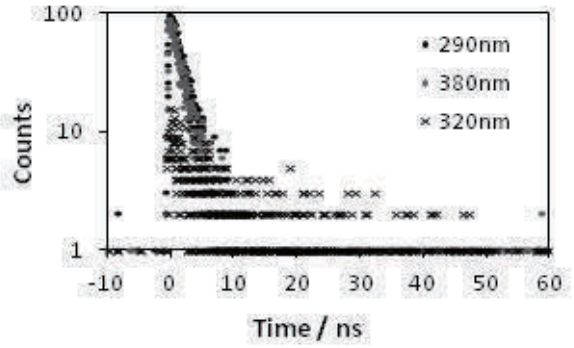

Fig. 3. Luminescence time profile at different wavelength.

BL7B

Electronic Status of Pr^{3+} in Glass Host by Characterizing Photoluminescence of Pr^{3+} Doped APLF Glass Scintillator

T. Nakazato[1], M. Tsuboi[1], K. Takeda[1], Y. Minami[1], T. Hori[1], T. Shimizu[1], R. Arita[1], K. Yamanoi[1], R. Nishi[1], Y. Shinzato[1], R. Sogi[1], N. Sarukura[1], H. Azechi[1], M. Cadatal-Raduban[2], T. Murata[3], S. Fujino[4], H. Yoshida[5], T. Suyama[6], K. Fukuda[6], A. Yoshikawa[7], N. Sato[8], H. Kan[8] and K. Kamata[8]

[1]*Institute of Laser Engineering, Osaka University, 2-6 Yamadaoka, Suita, Osaka 565-0871,Japan*
[2]*Centre for Theoretical Chemistry and Physics, Institute of Natural and Mathematical Sciences, Massey University, Albany, Auckland, 0632 New Zealand*
[3]*Kumamoto University, 2-39-1 Kurokami, Kumamoto 860-8555, Japan*
[4]*Kyushu University, 6-10-1 Hakozaki, Higashi-ku, Fukuoka 812-8581, Japan*
[5]*Ceramic Research Center of Nagasaki, 605-2 Hasami-cho, Higashisonogi-gun, Nagasaki 859-37, Japan*
[6]*Hamamatsu Photonics K.K., 325-6 Sunayama-cho, Naka-ku, Hamamatsu City, Shizuoka 430-8587, Japan*
[7]*Institute for Materials Research, Tohoku University, 1-1-2 Katahira, Aoba-ku, Sendai, Miyagi 980-8577, Japan*
[8]*Furukawa Co. Ltd., 2-6-1 Marunouchi, Chiyoda-ku, Tokyo 100-8370, Japan*

The realization of nuclear fusion is highly expected to satisfy the energy demand in the future. Fusion plasma diagnostics at higher plasma areal density than 3 g/cm^2 is one of the biggest breakthrough in nuclear fusion research. Scattered-neutron diagnostics [1] utilizing Pr^{3+}-doped $20Al(PO_3)_3$-80LiF (APLF+Pr) glass scintillator [2] is expected to achieve plasma areal density measurement in fusion core. APLF+Pr, which have high sensitivity for scattered neutrons and fast response time about 5.4 ns, is the key factor of the measure.

In this work, we report the luminescence properties of APLF+Pr at different Pr^{3+} concentrations (0.5mol%～3mol%).

We have measured Photoluminescence (PL) spectra and Photoluminescence Excitation (PLE) spectra of APLF+Pr at 30K, 100K, 200K, and 300K. The experiment was conducted at BL7B utilizing G2 grating. PL spectra are measured with excitation wavelength at 180nm, 200nm and 217 nm. The APLF+Pr samples, having Pr^{3+} density at 1mol%, and cut into 10 mm × 10 mm × 2.5 mm, were prepared. PL and PLE spectra of Pr^{3+}-doped $LiCaAlF_6$ (Pr:LiCAF) was measured as well for comparison.

The PL spectra of APLF+Pr excited by 180 nm radiation at 27 K, 100 K, 200 K and 300 K are shown in Fig. 1. 2 sharp peaks and 3 broad peaks have been found from 200 nm to 300 nm. The 2 peaks strongly depend on temperature and intensities decrease with increasing temperature. However the 3 broad peaks do not strongly depend on the temperature as compared with the 2 sharp peaks. The broad peaks of 227 nm, 236 nm and 261 nm are ascribe to 4f5d-$^5H_4$, 4f5d-$^5H_5$, and 4f5d-$^5H_6$, $^5F_2$ and $^5F_3$ respectively based on the results of Pr:LiCAF PL spectra. The sharp peaks of 253 nm and 273 nm are also ascribed to $^1S_0$-$^5F_4$ and $^1S_0$-$^1G_4$ respectively.

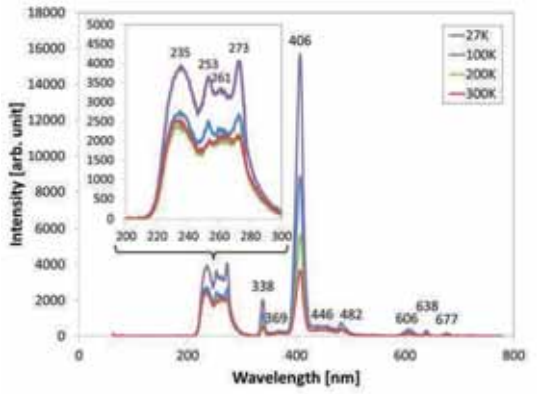

Fig. 1. PL spectra of APLF at various temperature.

[1] M. Moran *et al.*, Rev. Sci. Instrum. **75** (2004) 3592.
[2] T. Murata *et al.*, IEEE Trans. Nucl. Sci., **57** (2010) 1426.

BL8B

Photoelectric Emission from Ag/zinc-phthalocyanine Surface Under Near-UV Light Irradiation

S. Tanaka, K. Fukuzawa, T. Otani and I. Hiromitsu

Interdisciplinary Graduate School of Science and Engineering, Shimane University, 1060 Nishikawatsu, Matsue, Shimane 690-8504, Japan

The organic semiconductors have gained significant importance in the optoelectronic devices in the last decade. The electronic structure of the organic semiconductor has attracted interest from the view point of not only the basic science but also the practical application. For example, the electronic structure of the organic semiconductor/metal interface has an important role on the device performance of the organic solar cells [1]. Recently, we have studied the light irradiation effects on the electronic structure of the organic/metal and organic/organic interfaces to investigate the electronic structure under the working condition of the solar cells [2]. During the research, we found an anomalous photoelectric emission from the organic thin films with a surface treatment by metal deposition.

Figure 1 shows the photoelectric emission from the zinc phthalocyanine (ZnPc) film with Ag deposition under the 360 nm (= 3.44eV) laser irradiation. The nominal thickness of the ZnPc and Ag layer were 10 nm and 0.05 nm, respectively. The work function of Ag (~4.5 eV) and the ionization potential of ZnPc (~5.0 eV) are larger than the energy of the laser light. Thus, the present photoelectric emission could be an anomalous phenomenon at a particular condition of the organic/metal interface. The threshold of light energy for the photoelectron emission was approximately 3.3 eV.

To investigate the effect of the Ag deposition on the electronic structure of the sample surface, photoelectron spectroscopy was performed. The ZnPc layer was deposited on the indium tin-oxide (ITO) substrate by vacuum deposition at the preparation chamber. Ag was also deposited on the ZnPc layer by vacuum deposition. The thickness of the each material was monitored by quartz microbalance. The sample was transferred to the measurement chamber without breaking the vacuum. All the photoelectron measurements were carried out at room temperature. Figure 2 shows the variation of the photoelectron spectra of Ag deposited on the ZnPc substrate with increasing thickness. The highest occupied molecular orbital of ZnPc was shifted approximately 0.5 eV toward lower kinetic energies by the deposition of 0.5 nm of Ag. The secondary electron cutoff was also showed a corresponding shift. These results infer that the potential barrier for the photoelectric emission at the sample surface was decreased by the Ag deposition. However, the estimated value of the work function of the sample surface is much larger than the 3.3 eV. The shift of vacuum level is frequently observed at the organic/metal interface [3], although no anomalous photoelectric emission has been reported. The surface structure of the Ag/ZnPc sample was observed by atomic force microscope (AFM). The AFM images showed that Ag was deposited on the ZnPc surface with grain sizes of few nano meters. The structure of the Ag particles could be related to the reduction of the surface barrier potential. The fact that the anomalous photoelectric emission was suppressed at the thicker Ag region (Fig. 2. inset) could support this hypothesis.

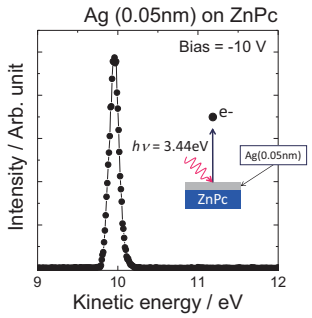

Fig. 1. Photoelectric emission from the Ag (0.05nm) /ZnPc (10nm) /ITO emitted by near-UV light irradiation ($h\nu$ = 3.44 eV). The sample was biased by −10 V to measure the electron with small kinetic energies.

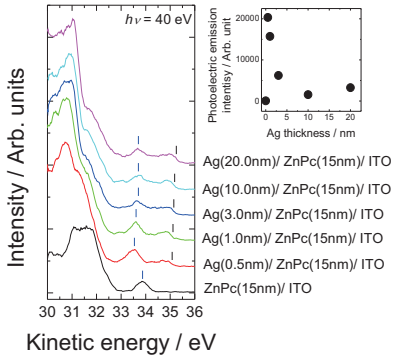

Fig. 2. Photoelectron spectra of ZnPc and Ag/ZnPc sample near the Fermi level. Inset: The Ag thickness dependence of the photoelectric emission intensity.

[1] S. Tanaka *et al.*, Appl. Phys. Lett. **97** (2010) 253306.
[2] S. Tanaka *et al.*, UVSOR Activity Report **39** (2012) 130.
[3] H. Ishii *et al.*, Adv. Mater., **11** (1999) 605.

BL8B

Does Polarity of the Giant Surface Potential Impacts Charge Transfer at Organic-Organic Interfaces?

H. S. Lim[1], Y. Ozawa[1], Y. Uragami[1], Y. Nakayama[2], Y. Noguchi[1,2] and H. Ishii[1,2]
[1]*Graduate School of Advanced Integration Science, Chiba 263-8522, Japan*
[2]*Center for Frontier Science, Chiba University, Chiba 263-8522, Japan*

Ito *et al.* reported spontaneous building up of the surface electric potential (giant surface potential; GSP) in vacuum deposited films of tris(8-hydroxyquinolinato) aluminum(III) (Alq_3) [1]. The origin of GSP can be attributed to a slight alignment of dipole moment of the molecules in average. The polarity of GSP in the case of Alq_3 is positive in increasing the film thickness.

We have reported how the existence/absence of GSP in an overlayer impacts the electronic nature at organic hetero-interfaces [2]. These works, however, are conducted on overlayers of non-GSP or positive GSP materials. In this context, an Alq_3-derivative tris(7-propyl-8-hydroxyquinolinato) aluminum(III) ($Al(7\text{-prq})_3$) is an interesting material because this reveals a negative GSP [3].

In this experiment, we investigated the influence of different GSP direction at organic interfaces of a N,N'-bis(1-naphthyl)-N,N'-diphenyl-1,10-biphenyl-4 ,40-diamin (α-NPD) film capped with the Alq_3 or $Al(7\text{-prq})_3$ overlayer.

Ito is used as substrate and is cleaned by ultrasonication in neutral detergent, isopropanol and acetone. 5nm-thick α-NPD layers were then deposited onto the ITO substrate. Alq_3 or $Al(7\text{-prq})_3$ was subsequently deposited onto α-NPD from 0.1nm to 10.0nm in a step-by-step manner. Ultraviolet photoelectron spectroscopy (UPS) was performed at BL8B at UVSOR. 40 eV of photon energy was used. -5 V bias was applied during secondary electron cutoff (SECO) measurement. The experiment is carried out at room temperature.

At the α-NPD/Alq_3 interface, the highest occupied molecular orbital (HOMO) peak of α-NPD (as well as the SECO position) moved with growing the thickness of Alq_3 by 0.1 eV to low kinetic energy side. This implies that deposition of Alq_3 induces downward band-bending in the α-NPD layers, namely charge transfer from α-NPD to Alq_3. As growing the Alq_3 overlayer further thicker, the SECO position shifted down proportionally to the Alq_3 thickness representing GSP.

α-NPD HOMO peak moved to low kinetic energy side also at the α-NPD/$Al(7\text{-prq})_3$ interface, yet the shifting value (~0.06 eV) was a little less than the case of the unsubstitued Alq_3. While SECO did not exhibit apparent shift in the thin coverage region, it moved to the high kinetic energy side in increasing the $Al(7\text{-prq})_3$ thickness, which can be attributed to GSP of the opposite polarity to the Alq_3 layers.

The present results implies occurrence of charge transfer from α-NPD to the overlayers irrespective of the polarity of GSP, which is contradicting to our previous proposition [2]. In order to figure out the electronic phenomena at the topical organic-organic interface, further systematic studies by altering the overlayer characteristics are highly anticipated.

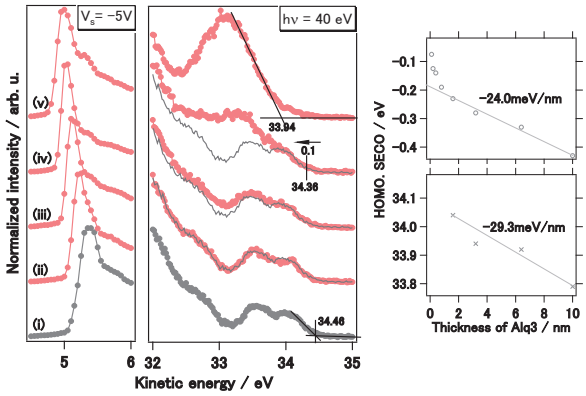

Fig. 1. UPS spectra of the Alq_3 [(i) : 0nm, (ii) : 0.1nm, (iii) : 0.4nm, (iv) : 1.6nm, (v) : 6.4nm] on α-NPD (5nm) interfaces. The gray line shows the spectra contribution of α-NPD, which is derived from a procedure described in Ref. [2].

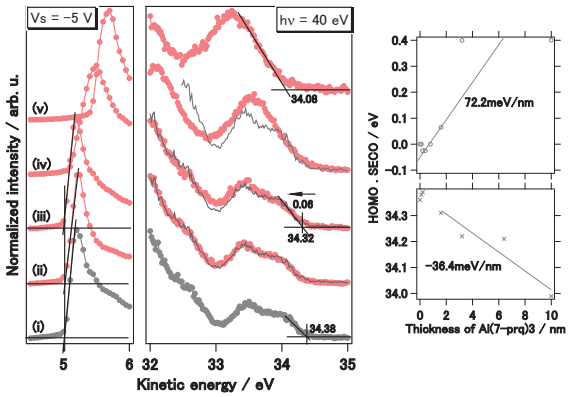

Fig. 2. UPS spectra of the $Al(7\text{-prq})_3$ [(i) : 0nm, (ii) : 0.1nm, (iii) : 0.4nm, (iv) : 1.6nm, (v) : 10.0nm] on α-NPD (5nm) interfaces.

[1] E. Ito *et al.*, J. Appl. Phys. **92** (2002) 7306.
[2] Y. Nakayama *et al.*, Organic Electrons **13** (2012) 2850.
[3] T. Isoshima *et al.*, *submitted.*